Title: Global ocean lipidomes show a universal relationship between temperature and lipid unsaturation

Authors: Henry C. Holm^{1,2}, Helen F. Fredricks¹, Shavonna M. Bent^{1,2}, Daniel P. Lowenstein^{1,2}, Justin E. Ossolinski¹, Kevin W. Becker¹†, Winifred M. Johnson^{1,2}‡, Kharis Schrage^{1,2}, Benjamin A. S. Van Mooy^{1*}

Affiliations:

5

10

15

20

25

¹Marine Chemistry and Geochemistry Department, Woods Hole Oceanographic Institution; Woods Hole, MA 02543, USA

²MIT-WHOI Joint Program in Oceanography/Applied Ocean Science & Engineering; Cambridge, MA, 02139, USA

†Present Address: GEOMAR Helmholtz Centre for Ocean Research Kiel, 24105 Kiel, Germany.

‡Present Address: Department of Chemistry and Biochemistry, University of North Carolina Wilmington, Wilmington, NC, 28403 USA

*Corresponding author. Email: bvanmooy@whoi.edu

Abstract: Global-scale surveys of plankton communities using 'omics' techniques have revolutionized our understanding of the ocean. Lipidomics has demonstrated potential to add further essential insights on ocean ecosystem function but has yet to be applied on a global scale. We analyzed 930 lipid samples across the global ocean using a uniform high-resolution accurate-mass mass spectrometry analytical workflow, revealing heretofore unknown characteristics of ocean planktonic lipidomes. Focusing on ten molecularly diverse glycerolipid classes we identified 1,151 distinct lipid species, finding that fatty acid unsaturation (i.e., number of carbon-carbon double bonds) is fundamentally constrained by temperature. We predict significant declines in the essential fatty acid eicosapentaenoic acid over the next century, which are likely to have serious deleterious effects on economically critical fisheries.

One-Sentence Summary: The first global ocean lipidome survey predicts a temperature linked decrease in the production of essential fatty acids.

Main Text: Lipids are a class of biomolecules produced and used by organisms from all Domains of life for energy storage, membrane structure, and signaling. Lipids make up 10-20% of the particulate organic carbon in the surface ocean where lipid production and inventories are greatest (1-3). For decades, oceanographers have used lipids as biomarkers of chemical and biological ocean processes (4). Despite robust research into their biogeochemistry, the combination of high-resolution mass spectrometry and downstream analytical tools has only recently allowed for comprehensive untargeted assessments of ocean lipids, on scales akin to surveys of other molecules such as nucleic acids and proteins (5–8). These new tools allow for the examination of hundreds to thousands of lipid species in a sample (the entirety of which is referred to as the 'lipidome') and presents the opportunity to holistically examine global factors affecting ocean lipid composition. Critically, marine plankton lipidomes are likely to change as a function of water temperature, dissolved nutrient concentration, salinity, community composition, and other properties of the surface ocean. Lipid membranes are a core part of cellular adaptions to environmental perturbations making lipidomics an important tool for understanding how planktonic communities in the surface ocean will shift due to climate change. *(9)*.

5

10

15

20

We present here a global-scale mass spectral dataset of planktonic lipidomes from 146 locations (Fig. 1A) with concurrent environmental metadata aggregated from seven oceanographic research cruises using standardized collection, preservation, and extraction methods. We used high performance liquid chromatography coupled with electrospray ionization high-resolution accurate-mass mass spectrometry (HPLC-ESI-HRAM-MS) to generate spectra from 930 lipid extracts from samples of planktonic particles retained on 0.22 μm pore-size membranes. Using the R coding language packages XCMS, CAMERA, and LOBSTAHS we searched this spectral dataset for the 10 dominant glycerolipid molecular classes

found in surface ocean particulate organic carbon (3,5, 10); our methods are not optimized for archaeal ether lipids and, thus, they are not included in our study. We retained 1,151 high-confidence intact glycerolipid annotations based on a combination of accurate mass, MS/MS spectra, adduct hierarchy, retention time, and positive/negative mode ionization characteristics (11). Lipids from each class were quantified using external curves of a representative lipid species. This approach has been validated by our lab for possible matrix effects via isotopically labeled internal standards (3).

5

10

15

20

We defined a lipid species's relative abundance as the mass percent of the total lipidome. Within the dataset, annotated glycerolipids displayed a unimodal distribution of abundances in log space with a small number of species making up the majority of the annotated lipid mass (Fig. 1B). We defined a lipid species's prevalence in the dataset as the percentage of samples in which the species was observed. Aside from an abundant subset of species present in >90% of the samples, prevalence across the dataset was fairly evenly distributed with a similar numbers of lipid species across lower percentages (Fig. 1C). Both these metrics were positively correlated, with higher-abundance lipids being more prevalent (Fig. 1D). Due to this relationship, the most abundant 247 of the 1,151 lipid species represented 90% of the total lipid mass. Of these highly abundant species, the majority are present in over 97% of samples. These metrics show that while molecular diversity in the ocean is relatively high, a comparably small number of highly common lipid species make up an outsized proportion of the mass. In total, this dataset represents over 600,000 identified peaks, but numerous other mass spectral features remained to be conclusively annotated. The raw spectral files are publicly available to serve as a resource for continued global ocean investigations in the vein of other large "-omics" based field studies.

Planktonic community lipidomes are affected by numerous environmental factors, e.g., nutrient availability (12), but here we report on the relationship between lipids and arguably the

most fundamental control on their composition: temperature (13). In a process called homeoviscous adaptation, organisms adapt to temperature-induced changes in membrane fluidity via shifts in the unsaturation level (i.e., number of double bonds) of their fatty acid moieties (13, 14). Our approach allowed us to examine the unsaturation state of individual glycerolipid classes in natural marine microbial communities across the oceans and differentiate class-internal temperature-induced shifts in unsaturation from shifts between different classes of distinct unsaturation (15). Throughout the ocean, the surface mixed layer typically has the highest lipid concentrations and the steepest latitudinal temperature gradients (1). Therefore, of the total 930 samples spanning 0-600 meters depth, we analyzed the 243 samples collected from the surface mixed layer (generally <40 m; Supplementary Materials).

5

10

15

20

In Figure 2, we present the saturation state in the mixed layer for four representative glycerolipid classes: 1) sulfoquinovosyl diacylglycerols (SQDG, Fig. 2A), glycolipids found almost exclusively in eukaryotic photosynthetic membranes and cyanobacteria (I0); 2) triacylglycerols (TAG, Fig. 2B), energy storage lipids from eukaryotic plankton, particularly those under nutrient stress, and the most abundant glycerolipid we identified (3); 3) diacylglyceryl trimethylhomoserines and diacylglyceryl hydroxymethyltrimethyl- β -alanines (DGTS/DGTA, Fig. 2C) betaine lipids important for adaption to nutrient stress with broad distribution among marine plankton (I6); and 4) phosphatidylethanolamines (PE, Fig. 2D) one of the major phospholipids found in membranes of heterotrophic bacteria (I0). Among these glycerolipid classes, we found temperature to be highly influential in structuring the relative abundance of fatty acid species; there is a clear transition from species with more unsaturated fatty acids at colder temperatures to fully saturated species (i.e., with only single bonds) at the warmest temperatures (Fig. 2A-D). These trends are also evident in all the other glycerolipid classes (Fig. S1) as well as the total aggregated lipidome of all glycerolipid classes (Fig. S2).

From this compositional information, we calculated a weighted average unsaturation state for each glycerolipid class. For all the glycerolipid classes, this weighted mean unsaturation derived from the composition was highly linearly correlated to water temperature (Fig. 2E-H, Table S1). All classes showed shifts along this gradient, a finding that is notable given both the unique inherent unsaturation states, taxonomic sources, and biochemical roles of each lipid class (e.g., SQDG in thylakoid membranes, DGTS/A and PE in cellular membranes, and TAGs in lipid bodies). There is considerable scatter in the data at low temperatures collected off the Antarctic coast, which might be due to mixing between truly planktonic organisms and plankton released from melting sea ice. Using a linear fit to the weighted mean unsaturation of all lipid classes combined we found the number of unsaturations nearly triples across the temperature range sampled (1.2 unsaturations per fatty acid at 29°C, versus 3.3 at -2°C; Fig. S2, Table S1).

5

10

15

20

Given the tight correlation of unsaturation to temperature within individual lipid classes across highly diverse geographic areas we suggest that this trend stems from a universal biophysical necessity to control cell membrane fluidity through homeoviscous adaptation. While our data are not sufficient to absolutely implicate this mechanism, the consistency of temperature as a predictor necessitates a fundamental biophysical explanation. Even when accounting for other environmental parameters (depth, salinity, nutrients, light, and time of year) in a linear multiple regressional analysis, temperature is the most powerful explanatory variable for membrane lipid unsaturation (Fig. S3; Supplementary Materials). The genetic ability for homeoviscous adaption appears widely distributed; in culture a wide range of marine phytoplankton taxa have been shown to change their membrane unsaturation with changing temperature (17,18, 19). Our study transects numerous ocean biomes and cannot resolve the question of whether temperature itself or links between temperature and planktonic community composition drive the trends we observe (20), but future 'omics' studies could shed light on this;

e.g., a metatranscriptomic survey of fatty acid desaturases. Indeed, it is striking that the relationship between temperature and unsaturation emerges from our dataset despite spanning such diverse and disparate planktonic communities, from the nutrient-depleted subtropical gyres to the highly-productive Antarctic coastal shelf.

5

10

15

20

Within the compositional changes seen in this dataset, we were interested in how the abundance of two specific unsaturated fatty acids - eicosapentaenoic acid (EPA 20:5n-3) and docosahexaenoic acid (DHA 22:6n-3) – shifted along the temperature gradient. These fatty acids are essential for nutrition in zooplankton and other higher trophic level organisms and must be obtained largely from their diet (21). Thus, phytoplankton are the primary source of these lipids in marine food webs (22). They are often referred to as long-chain essential fatty acids (LCEFA; along with alpha-linoleic acid 18:3n-3). Using diagnostic MS/MS spectra we were able to determine whether a mass feature contained a LCEFA based on characteristic fatty acid fragments in the intact polar glycerolipids, and we singled these out for further exploration (11). These fragments were difficult to deconvolute in TAGs, limiting definitive LCEFA detection, although species containing >5 double bonds are readily identifiable (Fig. S4). We found that the percent abundance of all polar glycerolipids (i.e., excluding TAGs) containing a LCEFA in the mixed layer varied between 3-36% and 6-28% for EPA and DHA, respectively (Fig. 3A, Fig. S5). Interestingly, while the percent abundance of EPA species showed a strong relationship to temperature, the correlations for lipids with DHA was weaker. In addition to affecting membrane fluidity, DHA has also been shown to affect permeability and membrane fusion more than other unsaturated species (23). Thus, our results may indicate that planktonic organisms use EPA for regulating membrane phase transition temperature and DHA for other functions.

Based on the strong relationship between planktonic EPA abundance and temperature, we sought to examine current geospatial patterns of this LCEFA. We fit a quadratic curve (R^2 =

10

15

20

0.91, p < 0.01, n = 239, Table S2) to %EPA versus temperature in mixed layer samples (Fig. 3A), and then used sea surface temperature data from the model inter-comparison project "CMIP6" to predict EPA abundance in the mixed layer (Fig. 3 B-D, modeled sea-surface temperature (SST) data from Kwiatkowski et al. 2020, 24). These temperature values come from 13 combined earth system models for historical and future temperature scenarios. Using modelmean annual average SST temperatures, we project that high latitude waters contain proportionally much more EPA than low latitude areas (Fig. 3B). Based solely on temperature we found the mean %EPA between $50^{\circ}-60^{\circ}$ latitude (19.4 \pm 3.41% for $50^{\circ}-60^{\circ}$ N, 22.9 \pm 2.61% for 50° - 60° S) to be four times the amount between 10° - 0° latitude ($5.8 \pm 0.32\%$ for 10° - 0° N,6.0 ± 0.46% for 10° -0°S). The seasonal range in these %EPA estimates could be even greater. To see how the upper and lower limits for this composition are likely to shift under future warming conditions, we generated %EPA maps using end-of-century SST conditions from SSP1-2.6 and SSP5-8.5 scenarios in the same multi-model (Fig. 3C-D, Fig. S6). SSP1-2.6 represents a high-mitigation scenario with low CO₂ emission, while SSP5-8.5 represents a higher CO₂ emission scenario. Under the SSP5-8.5 scenario, which, admittedly, is a worst-case scenario (25), the change in mean absolute %EPA (Δ %EPA_{abs} = %EPA_{future} - %EPA_{present}) was about -2% globally, but with some areas, particularly at higher latitudes, seeing a more drastic decrease of up to -7% Δ %EPA_{abs} (Fig. 3C). Interestingly, the largest relative changes (Δ %EPA_{rel} = $(\Delta\%EPA_{abs}/\%EPA_{present})$ x 100) are more geographically heterogeneous. For example, locations such as the Sea of Japan, Norway Sea, and Grand Banks lose up to a quarter of current EPA amounts (Fig. 3D). In addition, broad expanses of the western North Atlantic and western North Pacific also showed high relative decreases.

These observations of EPA's correlation to water temperature and future projections of its decline in abundance suggest global threats to this LCEFA's availability to higher-trophic levels

by the end of the century. Previous research in zooplankton (e.g., copepods) has shown that some species experience large swings in their LCEFA content when fed different diets that vary in prey fatty acid composition (26). Furthermore, the abundance of other precursor unsaturated fatty acids may further exacerbate stress from dietary LCEFA deficiency. Specifically, LCEFAstarved invertebrates may express desaturases and elongases act to synthesize LCEFAs from 18:3n-3, 18:3n-6 and 18:4n-3 fatty acids; this process is very inefficient compared to dietary EPA acquisition, and future decreases in the availability of these precursor fatty acids would place an additional biochemical tax on EPA production (27). In many fish species, diets that are poor in EPA lead to deleterious changes in immune function and therefore fitness (28). Thus, it is possible that declines in primary producer EPA levels could affect both nutritional value of fish (e.g., for human consumption) and their overall population stability. Specifically, fisheries in the aforementioned Sea of Japan, Norwegian Sea, and Grand Banks, as well as coastal fisheries around Alaska, eastern Russia, and the Peruvian upwelling system, all face high projected losses in relative EPA levels, adding another layer of stress to already projected shifts in fishery baselines (29). Additionally, the influences of projected warming and retreating ice cover on LCEFA shifts in the Arctic Ocean are unknown, but likely to be even more significant.

5

10

15

20

Better understanding of environmental factors and mechanisms affecting the planktonic community lipidomes is critical to projecting future changes in ocean ecosystem services. Previous studies have shown that rising temperatures are likely to cause poleward shifts in planktonic thermal niches (30). The expansion of gyres and permanent changes to phytoplankton communities may alter the fatty acid composition of a site year-round. However, with fatty acid unsaturation tied to rapid adaptation mechanisms, it is possible that marine heat waves could immediately affect phytoplankton lipids on much shorter timescales. This raises the possibility of transient events of decreased unsaturated lipid production with unknown effects on the life

histories of economically significant taxa or their prey. Given that the frequency and intensity of short-lived marine heat waves is projected to increase, more research is needed into how this may affect fatty acid unsaturation on daily to seasonal timescales (31).

References and Notes

- S. G. Wakeham, C. Lee, J. I. Hedges, P. J. Hernes, M. J. Peterson, Molecular indicators of diagenetic status in marine organic matter. *Geochimica et Cosmochimica Acta*. 61, 5363– 5369 (1997). doi:10.1016/S0016-7037(97)00312-8
 - B. Gašparović, A. Penezić, R. S. Lampitt, N. Sudasinghe, T. Schaub, Free fatty acids, tri-, diand monoacylglycerol production and depth-related cycling in the Northeast Atlantic. *Marine Chemistry*. 186, 101–109 (2016). doi:10.1016/j.marchem.2016.09.002
 - K. W. Becker, J. R. Collins, B. P. Durham, R. D. Groussman, A. E. White, H. F. Fredricks, J. E. Ossolinski, D. J. Repeta, P. Carini, E. V. Armbrust, B. A. S. Van Mooy, Daily changes in phytoplankton lipidomes reveal mechanisms of energy storage in the open ocean. *Nature Communications*. 9 (2018). doi:10.1038/s41467-018-07346-z
- J. P. Koelmel, M. P. Napolitano, C. Z. Ulmer, V. Vasiliou, T. J. Garrett, R. A. Yost, M. N. V. Prasad, K. J. Godri Pollitt, J. A. Bowden, Environmental lipidomics: understanding the response of organisms and ecosystems to a changing world. *Metabolomics*. 16, 56 (2020). doi:10.1007/s11306-020-01665-3
- 5. J. R. Collins, B. R. Edwards, H. F. Fredricks, B. A. S. Van Mooy, LOBSTAHS: An Adduct-Based Lipidomics Strategy for Discovery and Identification of Oxidative Stress Biomarkers. *Analytical Chemistry.* 88, 7154–7162 (2016). doi:10.1021/acs.analchem.6b01260

- 6. M. A. Saito, M. R. McIlvin, D. M. Moran, T. J. Goepfert, G. R. DiTullio, A. F. Post, C. H. Lamborg, Multiple nutrient stresses at intersecting Pacific Ocean biomes detected by protein biomarkers. *Science*. **345**, 1173–1177 (2014). doi:10.1126/science.1256450
- Tara Oceans Coordinators, S. Sunagawa, S. G. Acinas, P. Bork, C. Bowler, D. Eveillard, G. Gorsky, L. Guidi, D. Iudicone, E. Karsenti, F. Lombard, H. Ogata, S. Pesant, M. B. Sullivan, P. Wincker, C. de Vargas, Tara Oceans: towards global ocean ecosystems biology. *Nat Rev Microbiol.* 18, 428–445 (2020). doi:10.1038/s41579-020-0364-5

- 8. S. I. Cantarero, C. Henríquez-Castillo, N. Dildar, C. A. Vargas, P. von Dassow, M. Cornejo-D'Ottone, J. Sepúlveda, Size-Fractionated Contribution of Microbial Biomass to Suspended Organic Matter in the Eastern Tropical South Pacific Oxygen Minimum Zone. *Frontiers in Marine Science*. 7, 540643 (2020). doi:10.3389/fmars.2020.540643
- 9. I. Marinov, S. C. Doney, I. D. Lima, Response of ocean phytoplankton community structure to climate change over the 21st century: partitioning the effects of nutrients, temperature and light. *Biogeosciences*. 7, 3941–3959 (2010). doi:10.5194/bg-7-3941-2010
- 10. K. J. Popendorf, M. W. Lomas, B. A. S. Van Mooy, Microbial sources of intact polar diacylglycerolipids in the Western North Atlantic Ocean. *Organic Geochemistry*. **42**, 803–811 (2011). doi:10.1016/j.orggeochem.2011.05.003
 - 11. Materials and methods are available as supplementary materials at the Science website.
- 12. B. A. S. Van Mooy, H. F. Fredricks, B. E. Pedler, S. T. Dyhrman, D. M. Karl, M. Koblížek,
 M. W. Lomas, T. J. Mincer, L. R. Moore, T. Moutin, M. S. Rappé, E. A. Webb,
 Phytoplankton in the ocean use non-phosphorus lipids in response to phosphorus scarcity.
 Nature. 458, 69–72 (2009). doi:10.1038/nature07659

- 13. M. Sinensky, Homeoviscous Adaptation--A Homeostatic Process that Regulates the Viscosity of Membrane Lipids in Escherichia coli. *Proceedings of the National Academy of Sciences*. **71**, 522–525 (1974). doi:10.1073/pnas.71.2.522
- 14. J. Hazel, The role of alterations in membrane lipid composition in enabling physiological adaptation of organisms to their physical environment. *Progress in Lipid Research*. **29**, 167–227 (1990). doi:10.1016/0163-7827(90)90002-3

10

15

- 15. B. A. S. Van Mooy, H. F. Fredricks, Bacterial and eukaryotic intact polar lipids in the eastern subtropical South Pacific: Water-column distribution, planktonic sources, and fatty acid composition. *Geochimica et Cosmochimica Acta*. 74, 6499–6516 (2010). doi:10.1016/j.gca.2010.08.026
- 16. J. P. Cañavate, I. Armada, J. L. Ríos, I. Hachero-Cruzado, Exploring occurrence and molecular diversity of betaine lipids across taxonomy of marine microalgae. *Phytochemistry*. 124, 68–78 (2016). doi:10.1016/j.phytochem.2016.02.007
- 17. H. Jiang, K. Gao, Effects of Lowering Temperature During Culture on the Production of Polyunsaturated Fatty Acids in the Marine Diatom Phaeodactylum Tricornutum (bacillariophyceae)1. *Journal of Phycology*. **40**, 651–654 (2004). doi:10.1111/j.1529-8817.2004.03112.x
 - P. A. Thompson, M. Guo, P. J. Harrison, J. N. C. Whyte, Effects of variation in temperature.
 II. On the fatty acid composition of eight species of marine phytoplankton. *J Phycol.* 28, 488–497 (1992). doi:10.1111/j.0022-3646.1992.00488.x
 - 19. J. Pittera, J. Jouhet, S. Breton, L. Garczarek, F. Partensky, É. Maréchal, N. A. Nguyen, H. Doré, M. Ratin, F. D. Pitt, D. J. Scanlan, C. Six, Thermoacclimation and genome adaptation

- of the membrane lipidome in marine Synechococcus. *Environmental Microbiology*. **20**, 612–631 (2018). doi:10.1111/1462-2920.13985.
- 20. A. W. E. Galloway, M. Winder, Partitioning the Relative Importance of Phylogeny and Environmental Conditions on Phytoplankton Fatty Acids. *PLoS One.* **10** (2015), doi:10.1371/journal.pone.0130053

- 21. L. F. C. Castro, D. R. Tocher, O. Monroig, Long-chain polyunsaturated fatty acid biosynthesis in chordates: Insights into the evolution of Fads and Elovl gene repertoire.
 Progress in Lipid Research. 62, 25–40 (2016).doi:10.1016/j.plipres.2016.01.001
- 22. L. Ruess, D. C. Müller-Navarra, Essential Biomolecules in Food Webs. *Front. Ecol. Evol.***7**, 269 (2019).doi:10.3389/fevo.2019.00269
 - 23. W. Ehringer, D. Belcher, S. R. Wassall, W. Stillwell, A comparison of the effects of linolenic (18:3Ω3) and docosahexaenoic (22:6Ω3) acids on phospholipid bilayers. *Chemistry and Physics of Lipids*. 54, 79–88 (1990).doi:10.1016/0009-3084(90)90063-W
- 24. 1. L. Kwiatkowski, O. Torres, L. Bopp, O. Aumont, M. Chamberlain, J. R. Christian, J. P.
 Dunne, M. Gehlen, T. Ilyina, J. G. John, A. Lenton, H. Li, N. S. Lovenduski, J. C. Orr, J.
 Palmieri, Y. Santana-Falcón, J. Schwinger, R. Séférian, C. A. Stock, A. Tagliabue, Y.
 Takano, J. Tjiputra, K. Toyama, H. Tsujino, M. Watanabe, A. Yamamoto, A. Yool, T. Ziehn,
 Twenty-first century ocean warming, acidification, deoxygenation, and upper-ocean nutrient
 and primary production decline from CMIP6 model projections. Biogeosciences. 17, 3439–3470 (2020). doi:10.5194/bg-17-3439-2020
 - 25. Z. Hausfather, G. P. Peters, Emissions the 'business as usual' story is misleading. *Nature*. **577**, 618–620 (2020). doi: 10.1038/d41586-020-00177-3

- 26. A. J. Veloza, F.-L. E. Chu, K. W. Tang, Trophic modification of essential fatty acids by heterotrophic protists and its effects on the fatty acid composition of the copepod Acartia tonsa, *Marine Biology*. **148**, 779–788 (2006). doi:10.1007/s00227-005-0123-1
- 27. Ó. Monroig, N. Kabeya, Desaturases and elongases involved in polyunsaturated fatty acid biosynthesis in aquatic invertebrates: a comprehensive review. *Fish Sci.* **84**, 911–928 (2018). doi:10.1007/s12562-018-1254-x

- 28. M. T. Arts, M. T. Brett, M. J. Kainz, Eds., "Chapter 10, Health and Condition in Fish: The Influence of Lipids on Membrane Competency and Immune Response" in *Lipids in aquatic ecosystems* (Springer, Dordrecht; New York, 2009). pp. 237-255
- 29. W. W. L. Cheung, V. W. Y. Lam, J. L. Sarmiento, K. Kearney, R. Watson, D. Zeller, D. Pauly, Large-scale redistribution of maximum fisheries catch potential in the global ocean under climate change. *Global Change Biology*. **16**, 24–35 (2010). doi:10.1111/j.1365-2486.2009.01995.x
- 30. M. K. Thomas, C. T. Kremer, C. A. Klausmeier, E. Litchman, A Global Pattern of Thermal

 Adaptation in Marine Phytoplankton. *Science*. **338**, 1085–1088 (2012).

 doi:10.1126/science.1224836
 - 31. T. L. Frölicher, E. M. Fischer, N. Gruber, Marine heatwaves under global warming. *Nature*. **560**, 360–364 (2018).doi:10.1038/s41586-018-0383-9
- 32. C. de Boyer Montégut, Mixed layer depth over the global ocean: An examination of profile data and a profile-based climatology. J. Geophys. Res. **109**, C12003 (2004). doi:10.1029/2004JC002378

- 33. K. J. Popendorf, H. F. Fredricks, B. A. S. Van Mooy, Molecular Ion-Independent Quantification of Polar Glycerolipid Classes in Marine Plankton Using Triple Quadrupole MS. Lipids. 48, 185–195 (2013). doi:10.1007/s11745-012-3748-0
- 34. C. Kuhl, R. Tautenhahn, C. Böttcher, T. R. Larson, S. Neumann, CAMERA: An Integrated Strategy for Compound Spectra Extraction and Annotation of Liquid Chromatography/Mass Spectrometry Data Sets. Anal. Chem. **84**, 283–289 (2012).

- 35. M. Holčapek, M. Lísa, P. Jandera, N. Kabátová, Quantitation of triacylglycerols in plant oils using HPLC with APCI-MS, evaporative light-scattering, and UV detection. Journal of Separation Science. **28**, 1315–1333 (2005). doi:10.1002/jssc.200500088
- 36. B. C. O'Neill, C. Tebaldi, D. P. van Vuuren, V. Eyring, P. Friedlingstein, G. Hurtt, R. Knutti, E. Kriegler, J.-F. Lamarque, J. Lowe, G. A. Meehl, R. Moss, K. Riahi, B. M. Sanderson, The Scenario Model Intercomparison Project (ScenarioMIP) for CMIP6. Geosci. Model Dev. 9, 3461–3482 (2016). doi:10.5194/gmd-9-3461-2016
 - 37. R Core Team, R: A Language and Environment for Statistical Computing (R Foundation for Statistical Computing, Vienna, Austria, 2020; https://www.R-project.org/).
 - 38. H. Wickham, ggplot2: Elegant Graphics for Data Analysis (Springer-Verlag New York, 2016; https://ggplot2.tidyverse.org).
 - 39. C. O. Wilke, cowplot: Streamlined Plot Theme and Plot Annotations for "ggplot2" (2020; https://CRAN.R-project.org/package=cowplot).
- 40. A. Kassambara, ggpubr: "ggplot2" Based Publication Ready Plots (2020; https://CRAN.R-project.org/package=ggpubr).

- 41. R. K. Bauer, oceanmap: A Plotting Toolbox for 2D Oceanographic Data (2020; https://CRAN.R-project.org/package=oceanmap).
- 42. A. South, rnaturalearth: World Map Data from Natural Earth (2017; https://CRAN.R-project.org/package=rnaturalearth).
- 5 43. D. Pierce, ncdf4: Interface to Unidata netCDF (Version 4 or Earlier) (2019; https://CRAN.R-project.org/package=ncdf4).
 - 44. H. Wickham, tidyr: Tidy Messy Data (2021; https://CRAN.R-project.org/package=tidyr).
 - 45. H. Wickham, R. François, L. Henry, K. Müller, dplyr: A Grammar of Data Manipulation (2021; https://CRAN.R-project.org/package=dplyr).
- 46. RR1813 cruise data. DOI: 10.5067/SeaBASS/EXPORTS/DATA001
 - 47. LMG1810 cruise data. DOI: 10.7284/138731

- 48. AE1319 cruise data: DOI:10.26008/1912/bco-dmo.829797.1
- 49. KN210-04 cruise data: DOI:10.1575/1912/bco-dmo.481164.1
- 50. Van Mooy, B. A. (2012) CTD profiles from R/V Knorr cruise KN207-01 in the southern tip of Nova Scotia to Bermuda in 2012 (SargassoSeaLipids project). Biological and Chemical Oceanography Data Management Office (BCO-DMO). (Version 17 July 2012) Version Date 2012-07-17 http://lod.bco-dmo.org/id/dataset/3666 [3/25/2022]
- 51. Van Mooy, B. A., Dyhrman, S. T. (2015) CTD data from R/V Atlantic Explorer cruise
 AE1409 in the Western Tropical North Atlantic in 2014 (P Processing by Tricho project).
 Biological and Chemical Oceanography Data Management Office (BCO-DMO). (Version 23 October 2015) Version Date 2015-10-23. http://lod.bco-dmo.org/id/dataset/616342
 [3/25/2022]

Submitted Manuscript: Confidential Template revised February 2021

52. KM1709 data. http://scope.soest.hawaii.edu/data/mesoscope/mesoscope.html

53. Data and code for this paper are available on GitHub. DOI: 10.5281/zenodo.6390283

Acknowledgments: We would like to thank the captains and the crews of the RVs *Knorr*,

Atlantic Explorer, Kilo Moana, Roger Revelle, and Lawrence M. Gould as well as chief scientists

Michael Lomas (AE1319), Benedetto Barone and Tara Clemente (KM1709), Elizabeth

Kujawinski (KN210-4), and Deborah Steinberg (RR1813). Lester Kwiatkowski graciously

provided multi-model means of SST used here from multiple CMIP6 model projections. Kelsey

Perry and Marissa Small processed and prepared lipid samples from LMG1810. Jeremy

Tagliaferre collected samples on AE1319. Alyson Santoro and Pete Morton collected lipid

samples for the RR1813 cruise at sea. Fiona Hopewell collected lipid samples on cruise

KM1709.

5

10

15

20

Funding: The research was supported by grants to B.A.S.V.M, from:

National Science Foundation grant OCE-1031143

National Science Foundation grant OCE-1045670

National Science Foundation grant OCE-1059884

National Science Foundation grant OCE-1332898

National Science Foundation grant OPP-1543328

National Science Foundation grant OCE-1756254

National Science Foundation grant OCE-2022597

The Marine Microbiology Initiative division of the Gordon and Betty Moore Foundation

#5073

Submitted Manuscript: Confidential Template revised February 2021

Simons Foundation #721229

Author contributions:

Project administration: BASVM

Conceptualization: BASVM

Funding acquisition: BASVM 5

Data curation: HCH

Formal Analysis: HCH

Investigation: HCH, HFF, SMB, DPL, JEO, KWB, WMJ, JPT, KRS

Methodology: BASVM, HCH, HFF

Visualization: HCH 10

15

20

Writing – original draft: HCH, BASVM

Writing – review & editing: HCH, HFF, SMB, DPL, JEO, KWB, WMJ, KRS, BASVM

Competing interests: The authors declare that they have no competing interests.

Data and materials availability: All data from this analysis including lipid annotations and

applicable code is free to access on GitHub (53, version 1.0.1). The unprocessed mass spectra

for each lipid sample in this study is available via the *Metabolights* repository alongside

relevant environmental metadata for each sample (Permanent link:

https://www.ebi.ac.uk/metabolights/MTBLS2838). Modeled sea surface temperature values

from Kwiatkowski et al. are available online from the CMIP6 repository (24, DOE node:

https://esgf-node.llnl.gov/search/cmip6/). All CTD data is additionally available from BCO-

DMO (https://www.bco-dmo.org/) for four cruises (48-51), Rolling Deck to Repository (47)

Submitted Manuscript: Confidential Template revised February 2021

for LMG1810, on SeaBass for RR1813, and at the SCOPE collaboration website(52) for KM1709.

Supplementary Materials

Materials and Methods

5 Figs. S1 to S11

Tables S1 to S6

References (31–53)

Figure 1. Compositional structure of glycerolipid species in the global ocean lipidome. (A)

A map of dataset sampling locations with sites colored by deployment. (B) Histogram of lipid

species relative abundance in dataset. Relative abundance for each lipid species is the percent of

mass from all annotated lipids it makes up. (C) Histogram of lipid species prevalence in dataset.

Prevalence is defined as the percent of samples a lipid species is found in. (D) The relationship

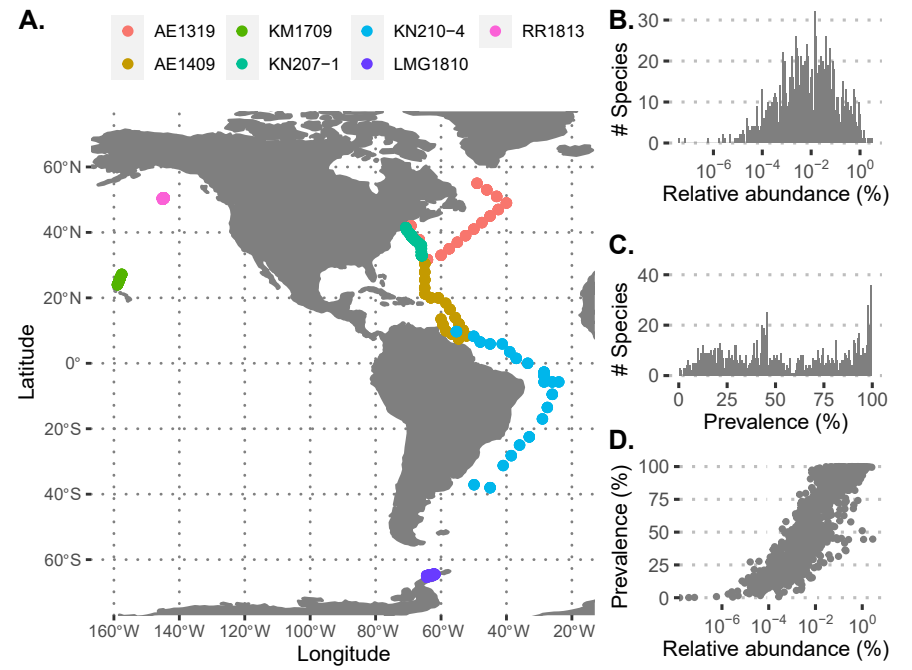
between prevalence and relative abundance for each lipid species.

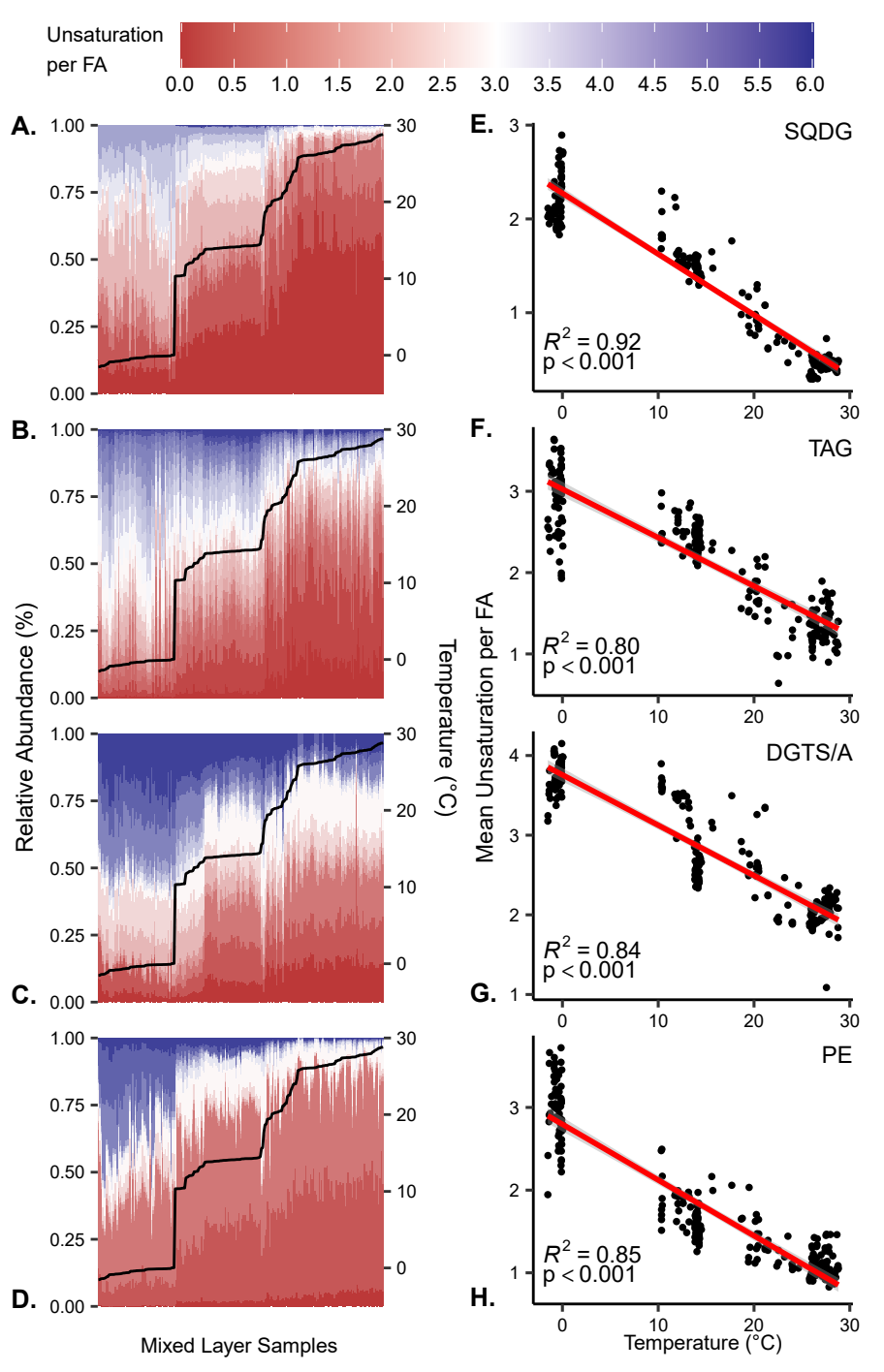
Figure 2. Mixed layer temperature is highly correlated with suspended fatty acid unsaturation. Four representative lipid classes are shown: a glycolipid (SQDG, A, E), an energy storage lipid (TAG, B, F), betaine lipids (DGTS/DGTA, C, G), and a phospholipid (PE, D, H). Identical figures for the other glycerolipids are provided in Supplementary Materials (Fig S1, S2). (A-D) Stacked bar plots show the relative abundance within each class of lipid species in mixed layer samples. Water temperature for each sample is shown with a black line plotted over the stacked bar plot (right axis). Samples are sorted from coldest to warmest along the x-axis. Lipid species are sorted from least (red) to most (blue) unsaturated along the y-axis and are colored to indicate the average number of unsaturations per fatty acid moiety on the glycerolipid. (E-H) Weighted mean number of unsaturations for each lipid class versus temperature among mixed layer samples. Red line shows linear fits; inset shows coefficient of determination for linear regression with ordinary least squares and p value from F-test (n = 242). Grey range shows 95% confidence interval of fit based on standard error.

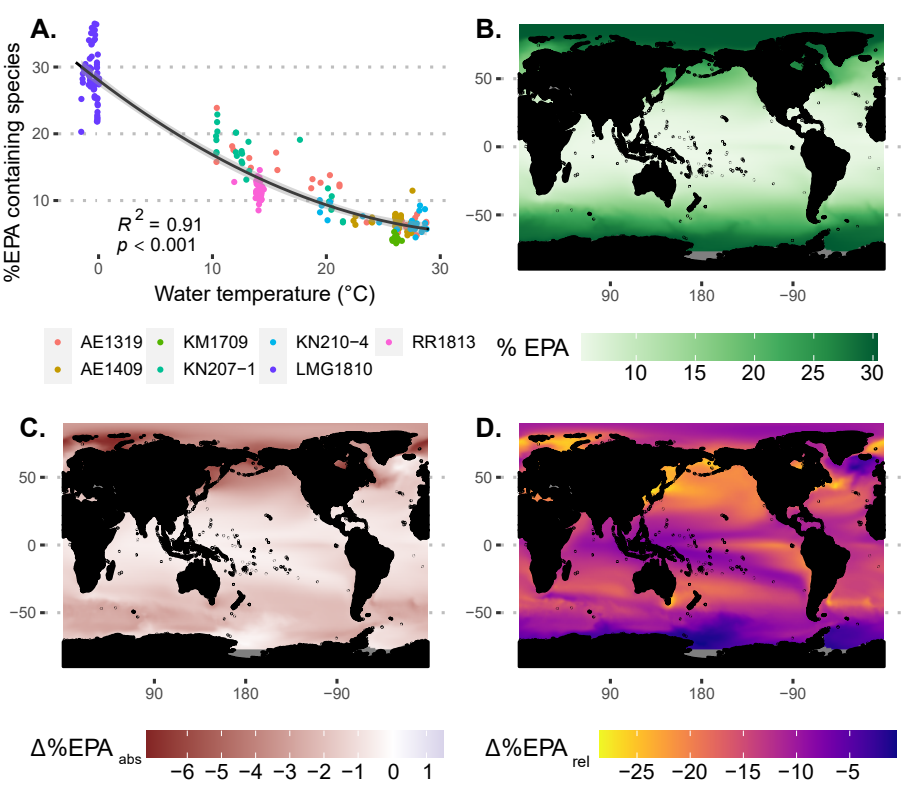
10

Figure 3. Current and future projections of EPA abundance based on water temperature shows loss under high-emission (SSP5-8.5) scenario. (A) Percent abundance of all polar glycerolipids containing EPA species (% EPA) in mixed layer samples verse temperature. Samples colored by deployment. Black line shows quadratic fit, grey area shows 99% confidence interval using standard error.(B) Current %EPA in mixed layer predicted using CMIP6 multimodel mean historical SST (1995-2014). (C) Change in absolute %EPA (Δ %EPA_{abs}) at end of century from today using SST under SSP5-8.5 scenario in the same models (2080-2099). (D) Projected relative loss of EPA (Δ %EPA_{rel}). Statistics for polynomial regression fit with ordinary least squares are shown in plot (n = 242, p values from F-test)

5









Supplementary Materials for

Global ocean lipidomes show a universal relationship between temperature and lipid unsaturation.

Henry C. Holm, Helen F. Fredricks, Shavonna M. Bent, Daniel P. Lowenstein, Justin E. Ossolinski, Kevin W. Becker, Winifred M. Johnson, Kharis Schrage, Benjamin A. S. Van Mooy

Correspondence to: bvanmooy@whoi.edu

This PDF file includes:

Materials and Methods Figs. S1 to S11 Tables S1 to S3, S5 Captions for Table S4, S6

Other Supplementary Materials for this manuscript include the following:

Table S4
Table S6

Materials and Methods

2 3

1.1 Sample collection

We collected the lipid fraction from suspended particulate organic matter on seven research cruises: KN207-1 on the R/V Knorr (April-May 2012), AE1319 on the R/V Atlantic Explorer (July-August 2013), KN210-04 on the R/V Knorr (March-April 2013), AE1409 on the R/V Atlantic Explorer (May 2014), KM1709 on the Kilo Moana (June-July 2017), RR1813 on the R/V Roger Revelle (August-September 2018), and LMG1810 on the R/V L.M. Gould (November 2018). For seawater sampling we used standard Niskin type bottles transferred to polycarbonate bottles before filtering. No permits are required for field collection of open ocean seawater. Seawater samples of 1-2 L were filtered at ~10 bar onto 0.22 μm hydrophilic Duropore filters (MilliporeSigma) immediately after water collection. Filters were folded, wrapped in aluminum foil, then flash frozen in liquid nitrogen (-196 °C) until extraction. We used processed CTD data to both measure water samples in-situ temperature at time of collection and assess mix layer depth with density. For each cast, the mixed layer depth was calculated as the first depth where the change in density from 5 meters exceeded 0.1 kg/m³. This definition is within the range of widely used mixed layer depth definitions (32).

From the available compiled CTD metadata we additionally complied concurrent measurements of chlorophyll-a fluorescence (mg m⁻³), photosynthetically available radiation (PAR; μE m⁻² s⁻¹), and dissolved nitrogen and phosphate (NO₃+NO₂, PO₄). Not all measurements were available for every cruise and lipid sample. Chlorophyll-a fluorescence was measured with an *in-situ* fluorometer on all deployments accept RR1813 where discrete sampling was performed on a ship-based Turner brand fluorometer. Due to the aggregate nature of the dataset, variable yet intercomparable methods were used for determination of dissolved nutrients. Full methods for each deployment can be found at their online repository (46-52).

1.2 Lipid Extraction

We performed lipid extraction using a modified Bligh and Dyer method detailed in Popendorf et al. 2013 (33). First, frozen filters were combined with 0.8 mL of phosphate buffered saline (PBS, 137 mM sodium chloride, 2.7 mM potassium chloride, 11.9 mM phosphate, pH = 7.4; Fisher Scientific), 2 mL of methanol, and 1 mL of dichloromethane (DCM) in glass centrifuge vials. An internal standard 2,4-dinitrophenyl- phosphatidylethanolamine (DNP-PE, Avanti Polar Lipids, Inc.) in methanol was added to track recovery and retention time movement (20 µL, concentration 65.6 µM). In addition, each extract received 10 µL of 1.5 mM butylated hydroxy toluene to each sample to resist sample oxidation. Following this step, samples are placed in a Fisher Scientific FS110 sonicator bath for 10 minutes. A final 1 mL of DCM and 1 mL of PBS is added to each sample causing phase separation. To aid this process, samples are centrifuged at 515 ×g for 5 minutes in an Eppendorf 5702 centrifuge. After this separation step, we retained the organic phase on the bottom of the vial in 2 mL HPLC vials. We stored these total lipid extracts under argon gas and frozen (-20 °C) to limit the possibility of oxidation before analysis. For each analysis we used 100 µL of this total extract, evaporated the DCM solvent with nitrogen gas, and resuspended the sample in 100 µL 70:30 acetonitrile:isopropanol by volume. Samples were again stored under argon gas before HPLC-ESI-HRAM-MS analysis.

1.3 HPLC-ESI-MS Lipid Analysis

High performance liquid chromatography (HPLC) analysis was carried out using reverse phase chromatography on an Agilent 1200 HPLC (Agilent Technologies). The HPLC settings are identical to the one described in Collins et al. 2016 (5). The HPLC system consisted of an autosampler, binary pump, column compartment, and diode array detector. This was fed into a Thermo Q-Exactive Orbitrap high resolution mass spectrometer (ThermoFisher Scientific) for high resolution/ accurate mass electrospray ionization mass spectral analysis (HRAM-ESI-MS). Batches of samples were briefly stored at 4 °C in the autosampler before analysis. The liquid chromatography was as follows: The aqueous Eluent 'A' consisted of MilliQ water with 1% 1 M ammonium acetate and 0.1% acetic acid. The organic Eluent 'B' consisted of 70% acetonitrile, 30% isopropanol with 1% 1 M ammonium acetate and 0.1% acetic acid. A 20 µL aliquot of the sample was injected at the start of the 40 minute program. For each run the system is kept at a flow rate of 0.4 mL per minute first with a gradient of 45% to 35% eluent 'A' between minutes 1-4, 25% to 11% eluent 'A' between minutes 4-12, 11% to 1% between minutes 12-15, then holding 1% eluent 'A' from 15-25 minutes. Lastly, eluent 'A' is returned to 45% for minutes 30-40 to clear the column (Table S3). The ESI source was set to 4.5 kV positive / 3.0 kV negative with a capillary temperature of 200°C and ESI probe temperature of 350 °C. Twenty-five samples were found to be compromised due to an ESI source needle blockage and their spectra were removed from further analysis as lipid responses were not adequate for compositional determination.

The Q-Exactive method was programmed to acquire data as follows: Positive-ion full-scan (200-1500 m/z) followed by data-dependent MS/MS (MS²) scans of the top 3 most abundant ions. Then, negative-ion full-scan (200-1500 m/z) followed by data-dependent MS² scans of the top 3 most abundant ions. Dynamic exclusion settings were such that an ion was excluded from further MS² analysis for 10 seconds, giving a broader depth of MS² data whilst also giving MS² spectra at the start, apex and end of a chromatographic peak. Masses for MS² were isolated with a 4 m/z window and fragmented with a stepped (normalized) collision energy of 30, 50 and 80. Common background ions were added to an exclusion list. Real time mass calibration was enabled with lock masses of 536.16591 (C₁₄H₄₆NO₇Si₇⁺, cyclodimethylpolysiloxane, [M+NH₄⁺]) and 297.27990 (C₁₉H₃₇O₂⁻, *n*-nonadecanoic acid [M-H⁻]) were maintained at a low but consistent abundance in the source by placing a silicone autosampler vial septum and a glass vial of nonadecanoic acid in the source during analysis.

1.4 Lipid Identification

We used the R package and pipeline LOBSTAHS to assist in the detection of lipids from a total ion chromatogram (5). Using multiple criteria, this pipeline allows for high-throughput screening of the entire sample dataset for thousands of unique lipid species. Samples were run through this lipid detection pipeline in four batches (Group 1: KN207-1, AE1319, KN210-04, AE1409, Group 2: KM1709, Group 3: RR1813, Group 4: LMG1810) with identical parameters based on when they were analyzed via HPLC-ESI-MS. Validated annotations from each of the four batches were joined after analysis. First, mass features were detected, grouped, and retention time aligned across samples using the popular R package XCMS. Relevant parameters and settings used for peak detection, grouping, and retention time alignment can be found in Table S4. The 'centWave' algorithm was used for peak detection across samples. Mass features were grouped with the 'density' method and peaks found in less than 2% of samples were not considered for analysis. Mass features were aligned using the 'loess' method using features found in greater than 90% of samples. For each of these features, when a peak was not initially detected in a sample by the centWave algorithm, the retention time region in the sample was integrated from the raw data.

This allows the integration of peaks present in a sample but not detected by the peak detection algorithm.

From here, the package CAMERA was used to group features into compound "pseudospectra". Pseudospectra are a group of all mass features, adducts and isotopes, which are likely to originate from the same compound (34). This allows for isotope peaks and adducts deriving from the same compound to be annotated as such. Settings for CAMERA analysis can also be found in Table S4. Finally, we used LOBSTAHS to screen pseudospectra against a database of lipid species using adduct hierarchy and accurate mass. A 2.5 ppm mass difference from the assignment was used as a hard threshold to retain any assignment in raw output. Only unoxidized annotations for the ten glycolipid classes found in Table S1 were considered for further analysis.

Final annotations were manually confirmed and subset from raw LOBSTAHS output using accurate mass, MS² spectra, adduct hierarchy, positive-negative ionization, and retention time patterning. For 301 of these annotations representing 67% of the total quantified mass, a MS² scan with diagnostic fragments confirming the annotation was seen giving the annotation high confidence. See Fig. S7 for lipid class specific diagnostic spectra. Additionally, 300 annotations representing 52% of the mass were designated "C2a" by LOBSTAHS adduct hierarchy screening in at least one of the four batches. This highest designation means that the pseudospectrum for the compound contained all possible adducts in the database and contained them in the theoretical order of abundance. We compared the ionization of the major adduct in positive and negative mode for each annotation to verify similar peak shapes. Since triglycerides did not ionize in negative mode this metric was not used to assist triglyceride identification. However, for 432 membrane lipid annotations representing 95% of the membrane lipid mass, the theoretically highest abundant adduct of the compound was matched between the two modes in a representative sample. All 1051 annotated features have an accurate mass less than or equal to 2.5 ppm of their theoretical m/z and fit within the expected fatty acid unsaturations/carbon retention time series of higher confidence annotations.

Annotated features were identified as a LCEFA (EPA and/or DHA) containing feature based on diagnostic MS^2 spectra. Since some mass features presented a mix of fatty acid fragments, any mass feature with a positive or negative MS^2 scan that contained a LCEFA fragment in at least one representative sample was designated an EPA or DHA containing feature. A diagnostic MS^2 was not available for every lipid species. On average, 6.2 ± 3.4 % of possible EPA containing annotations and 5.3 ± 3.0 % of possible DHA annotations by mass had no diagnostic MS^2 scan (Fig. S8). Intact TAG species presented a particular obstacle for fatty acid moiety detection; fully saturated and monounsaturated TAG species yielded good diagnostic fragments while more unsaturated (and especially polyunsaturated species) yielded no diagnostic fatty acid fragments (Fig. S7 M-N). This likely resulted from polyunsaturated species being more sensitive to fragmentation at the same collision energies. However, the lack of diagnostic fragments in this case limited our determination of which TAG species with >5 and 6 total unsaturations contained a LCEFA moiety. Thus, TAG species were excluded from the LCEFA analysis and our %EPA and %DHA values reflect only the mass percent of LCEFA species from the intact membrane lipid pool.

1.5 Quantification and Correction

Lipid peak areas were quantified to picograms on-column using representative linear standard curves run with identical LC-MS conditions on the same system. Table S5 details the

standards used to quantify each class. Quantification of feature peaks areas is necessary to correct for large differences in ionization response between lipid classes. Using curves based on a single representative lipid species for each class, we assumed that all lipid species from that class had the same response factor. This has been validated by previous work in our lab that shows saturated and unsaturated species vary less than 20% (33). While a relatively small change in ionization response has been observed between saturated and fully saturated membrane lipids of the same class, triglycerides have been shown to have a variable response based on their saturation and size (, 35). Due to this, TAG species were corrected with individual response factors based on their equivalent carbon number (ECN, Fig. S9). ECN is defined as the number of carbons (C) in the fatty acid chains minus two times the number of unsaturations (U) giving the equation:

$$ECN = C - 2 * U$$

Two fourth-order polynomial functions were fit to this plot in order to predict the response factor of any TAG from its ECN. Fit 1 uses TAG standards with ECN of 24-42 and Fit 2 uses TAG standards with ECN of 42-57. TAGs with ECN < 42 were corrected with Fit 1, and those with ECN \geq 42 with Fit 2. Final totals in each sample were subtracted with field blanks from each cruise with the following exceptions where field blanks were not available: samples from KN207-1 were blank corrected with field blanks from KN210-4 and samples from KM1709 used solvent extraction blanks processed with these samples in the lab. In subsequent analysis, the relative abundance of each lipid compound was used; that is the quantified picograms of a lipid species divided by the total mass of lipids in the sample.

1.6 Weighted Mean Calculations

A weighted arithmetic mean using the percent abundance of each lipid species was used to calculate the mean unsaturation per fatty acid on a lipid species within a sample (Fig. 2 F-I). When calculating the weighted mean unsaturation of a lipid class, percent abundance was calculated only using the lipids from that class. We calculated the weighted mean for each sample as:

$$WMU = u_0 w_0 + u_1 w_1 + u_2 w_2 \dots u_n w_n$$

where WMU is the weighted mean unsaturation per fatty acid, " u_n " is the amount of unsaturations on a given lipid species per fatty acid, and weight " w_n " is the percent abundance of all lipid species with " u_n " amount of unsaturations. Since " w_n " are percent abundances, all the weights in the calculation sum to 1. A simple linear regression ($y = b_2 x + b_1$) fit with ordinary least squares was used to compare the change in weighted mean unsaturation within each lipid class to temperature (Fig.2, Fig. S1), among all membrane lipid classes grouped together, and all lipid classes grouped together including TAGs (Fig. S2, Table S1). Linear regression was selected for effective comparison between classes and generally explained the observed trends well (all $R^2 > 0.7$), however, it is worth noting that to our knowledge there is no biochemical necessity for this response to strictly be linear.

1.7 Fatty Acid Abundance Projections

We evaluated the future abundances of EPA and DHA in membrane lipids by fitting an ordinary least squared model to the abundance of species containing these fatty acids (%EPA/%DHA, see section 1.4) with *in situ* temperature at the time of collection. A quadratic

function $(y = b_3 x^2 + b_2 x + b_1)$ was chosen to fit the data due to the residuals of a linear fit verses the fitted values for %EPA showing a convex shape. We then transformed three 1°x1° gridded maps of sea surface temperature generated by CMIP6 multi-model means to LCEFA percent abundances by applying the fitted quadratic function (Table S2). For full methods on generation of the modeled sea surface temperature values see Kwiatkowski et al. 2020 (24). In brief, 13 CMIP6 models with one ensemble member per model were averaged with equal weight given to each model. All historical simulations were made over 1850-2014 with mean values of 1995-2014 serving as the baseline period against which change is expressed. These models use emissions and land-use scenarios called 'Shared Socioeconomic Pathways' deriving from the Scenario Model Intercomparison Project. We used modeled mean historical sea surface temperature (SST) from 1995-2014 as our current ocean SST. We used scenarios SSP-2.6 and SSP5-8.5 as low and high emission scenarios respectively (Fig. 3, Fig. S6). Complete information about the assumptions and emissions in both scenarios can be found in O'Neill et al. 2016 (36). The absolute change for future scenarios in percent EPA (Δ %EPA_{abs}) and change in EPA relative to current conditions (Δ %EPA_{rel}) was calculated as:

$$\Delta\%EPA_{abs} = future\%EPA - present\%EPA$$

202
$$\Delta\%EPA_{rel} = \left[\frac{\Delta\%EPA_{abs}}{present\%EPA}\right] * 100$$
203

where 'present %EPA' is the percent EPA at a location as predicted by mean historical SST from 1995-2014 and 'future %EPA' is the percent EPA at a location as predicted by mean future SST from 2080-2099 in both scenarios respectively.

1.8 Multiple Linear Regression Model

We employed a multiple linear regression (MLR) model to examine the explanatory effects of other environmental variables on unsaturation along with temperature. Additionally, this approach allowed us to examine the significance of temperature as a predictor while accounting for the effects of other variables. From the available CTD metadata we used temperature, Chl-a fluorescence, depth, salinity, photosynthetically available radiation (PAR), and dissolved nitrogen (NO₃+NO₂) as independent variables. Additionally, we included the number of days since the summer solstice as a proxy for seasonality. Using these variables, we ran three MLR models to predict the weighted mean unsaturation of all membrane lipids combined, %EPA containing lipids, and %DHA containing lipids. Complete metadata was not available for every variable for every deployment. Therefore, the models were run using samples with complete observations within the mixed layer (n=112). Dissolved phosphate was excluded from the multiple linear regression as it displayed high collinearity with dissolved nitrogen leading to variable inflation factors (VIF) greater than 10. In cases where NO₃+NO₂ was below the detection limit the value was substituted for half the limit of detection for the analysis (2-10 nM). Both dissolved NO₃+NO₂ and fluorescence were square root transformed to improve linearity. Lastly, all variables, including dependent variables, were standardized by subtracting the mean and dividing by the standard deviation of the variable (z-score) to compare standardized coefficients. VIF were less than 10 for are variables in the final model

1.9 Additional Software Employed

All statistical analysis and visualization were performed in R (37) with the following packages: ggplot2, cowplot, and ggpubr (38-40) for figure plotting, oceanmap and rnaturalearth (41-42) for generating ocean maps, ncdf4 (43) for reading of ocean temperature data, tidyr and dplyr (44-45) for data formatting.

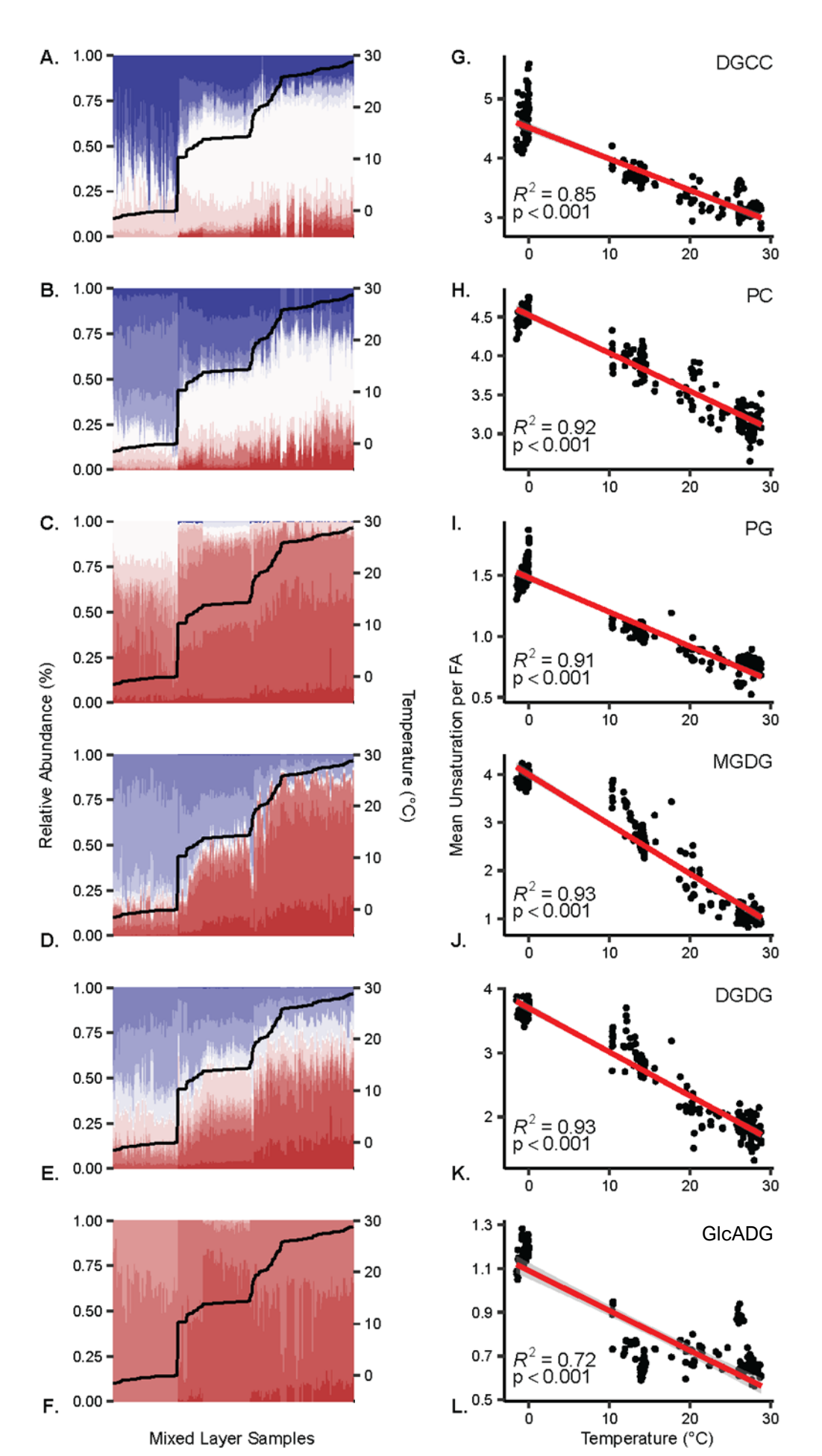


Figure S1.

Trends in unsaturation verses temperature for glycerolipid classes. Temperature trends for remaining lipid classes not plotted in the main text are shown above: DGCC (A, G), PC (B, H), PG (C,I), MGDG (D, J), DGDG (E,K) GlcADG (F, L). Stacked bar plots (A-F) show the relative abundance within each class of lipid species in mixed layer samples. Samples are sorted from coldest to warmest along the x-axis. Lipid species are sorted from least (red) to most (blue) unsaturated along the y-axis and are colored to indicate the average number of unsaturations per fatty acid moiety on the glycerolipid. Water temperature for each sample is shown with a black line plotted over the stacked bar plot (right axis). (G-L) Weighted unsaturation for each lipid class versus temperature among mixed layer samples. Red line shows linear fits; inset shows coefficient of determination for linear regression fit with ordinary least squares and p value from F-test (n = 242). Grey range shows 95% confidence interval of fit based on standard error.

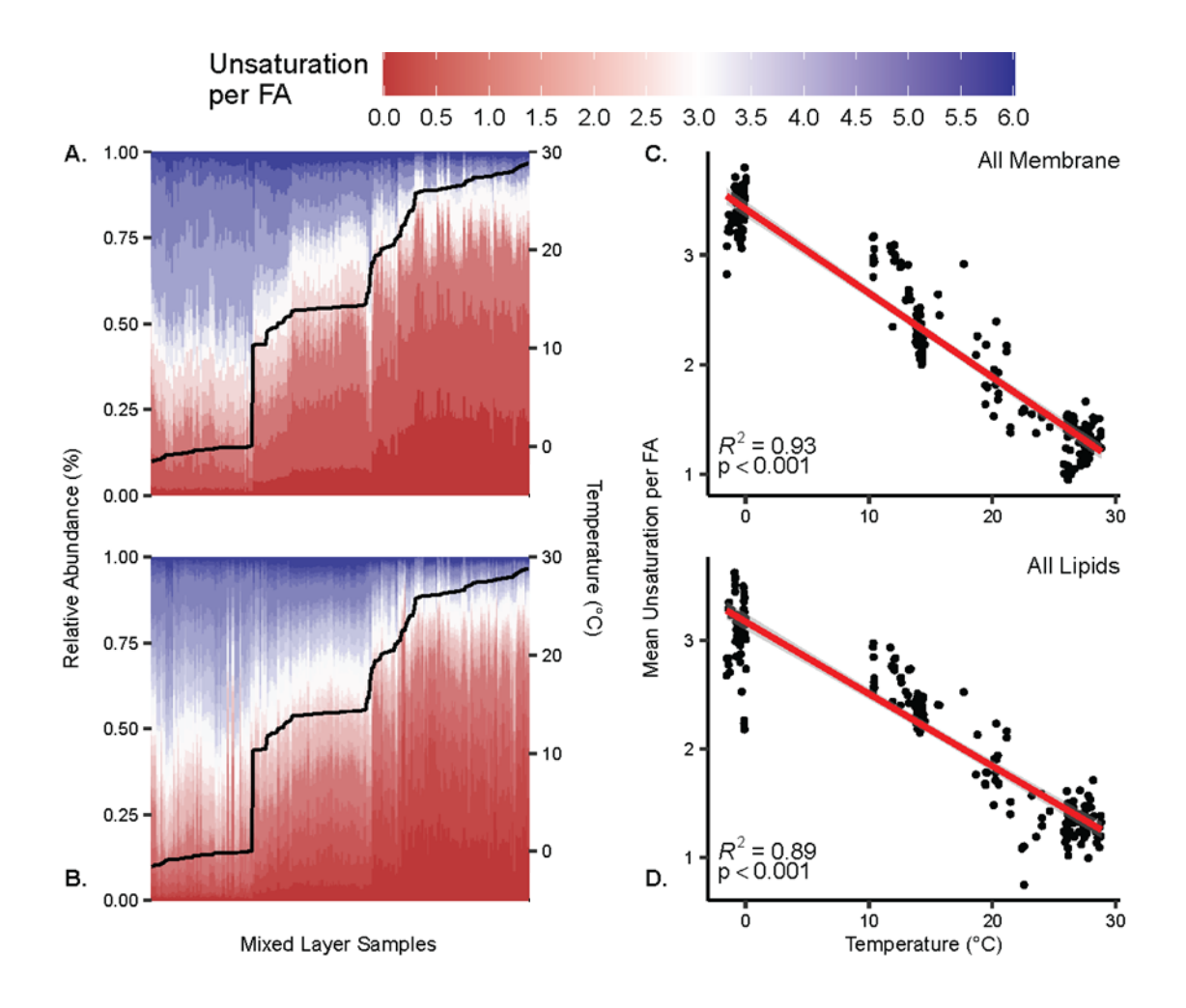


Figure S2. Trends in unsaturation verses temperature for combined glycerolipid classes. Temperature trends are shown for all membrane glycerolipids combined (A, C) and all lipids including TAGs (B, D). Stacked bar plots (A-B) show the relative abundance within each class of lipid species in mixed layer samples. Samples are sorted from coldest to warmest along the x-axis. Lipid species are sorted from least (red) to most (blue) unsaturated along the y-axis and are colored to indicate the average number of unsaturations per fatty acid moiety on the glycerolipid. Water temperature for each sample is shown with a black line plotted over the stacked bar plot (right axis). (G-L) Weighted mean unsaturation for each lipid class versus temperature among mixed layer samples. Red line shows linear fits; inset shows coefficient of determination for linear regression fit with ordinary least squares and p value from F-test (n = 242). Grey range shows 95% confidence interval of fit based on standard error.

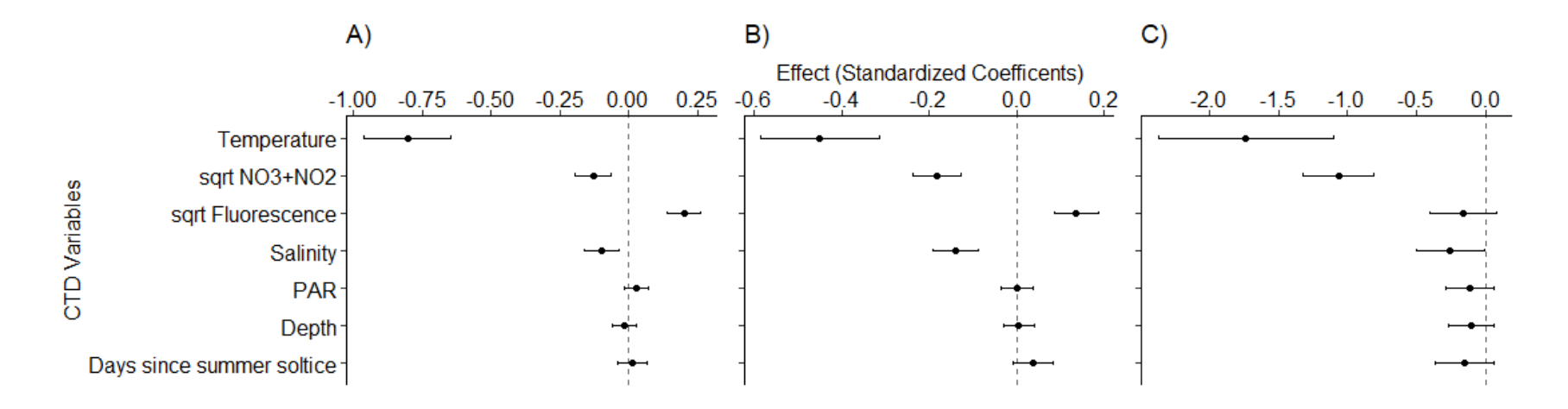


Figure. S3.

Effects plots showing standardized coefficients of multiple linear regression analysis. Coefficients for environmental CTD predictor variables modeling (A) weighted mean unsaturation of all membrane lipids (adjusted $R^2 = 0.93$, p < 0.01, n=114) (B) percent EPA containing lipids (%EPA, adjusted $R^2 = 0.89$, p < 0.01, n=114) and (C) percent DHA containing lipids (%DHA, adjusted $R^2 = 0.58$, p < 0.01, n=114). Effect is measured as the change in standard deviations of the dependent variable given a one standard deviation change in the predictor variable. Holding all other variables constant, all three dependent variables were most sensitive to changes in temperature. All models fit with ordinary least squares; p value indicates F-test for the overall model. See Table S6 for full model output.

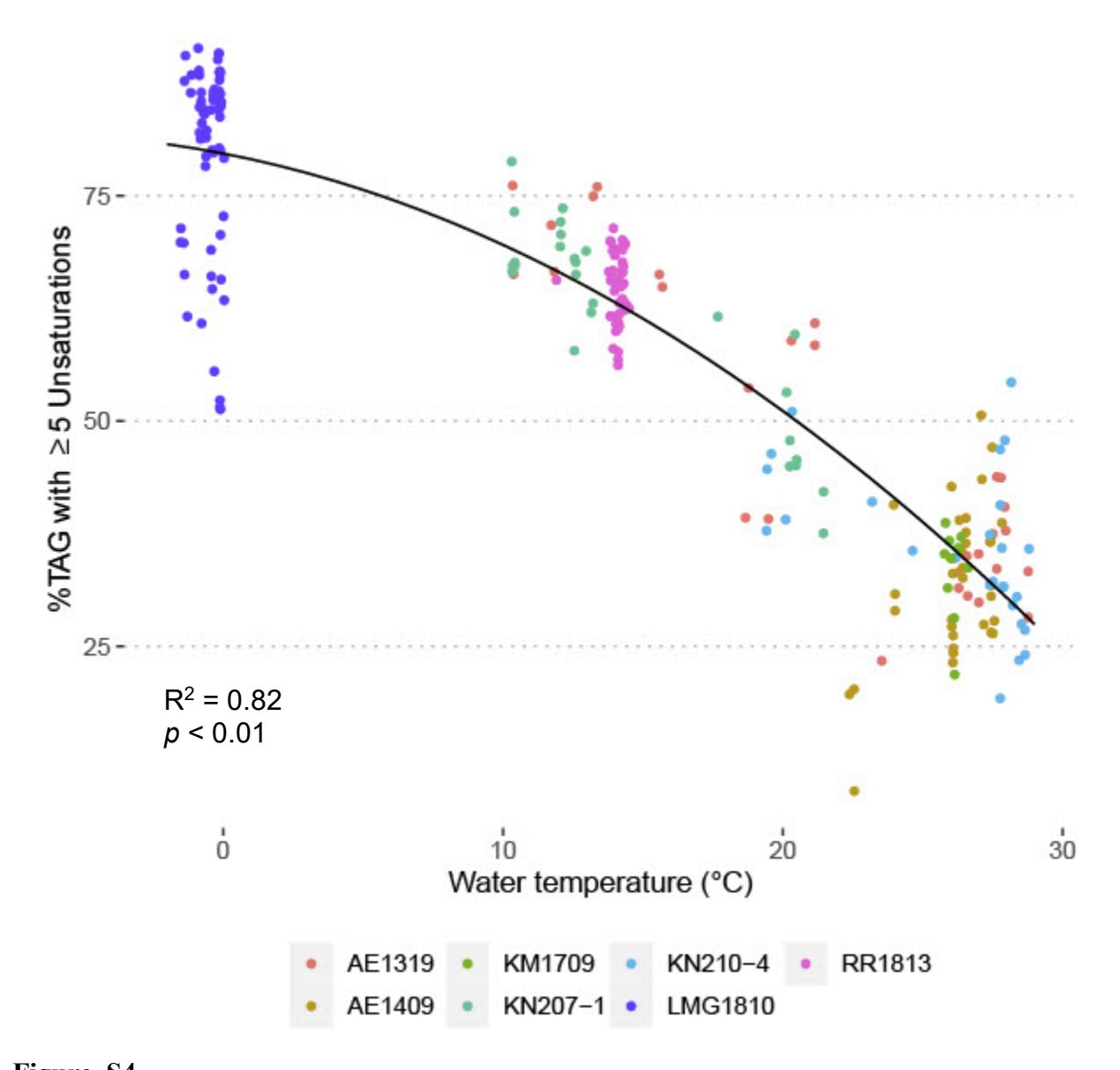


Figure. S4. Abundance of TAG species \geq 5 unsaturations verses temperature in mixed layer samples. The y-axis shows the combined abundance of all TAG species that have annotations with at least five unsaturations across their three fatty acid moieties. Seawater temperature at the time of sample collection is shown on the x-axis. Color denotes the deployment on which the sample was collected; Black line shows fitted values. Statistics for polynomial regression fit with ordinary least squares are shown in plot (n = 242, p values from F-test). (See Table S2 for full fit parameters).

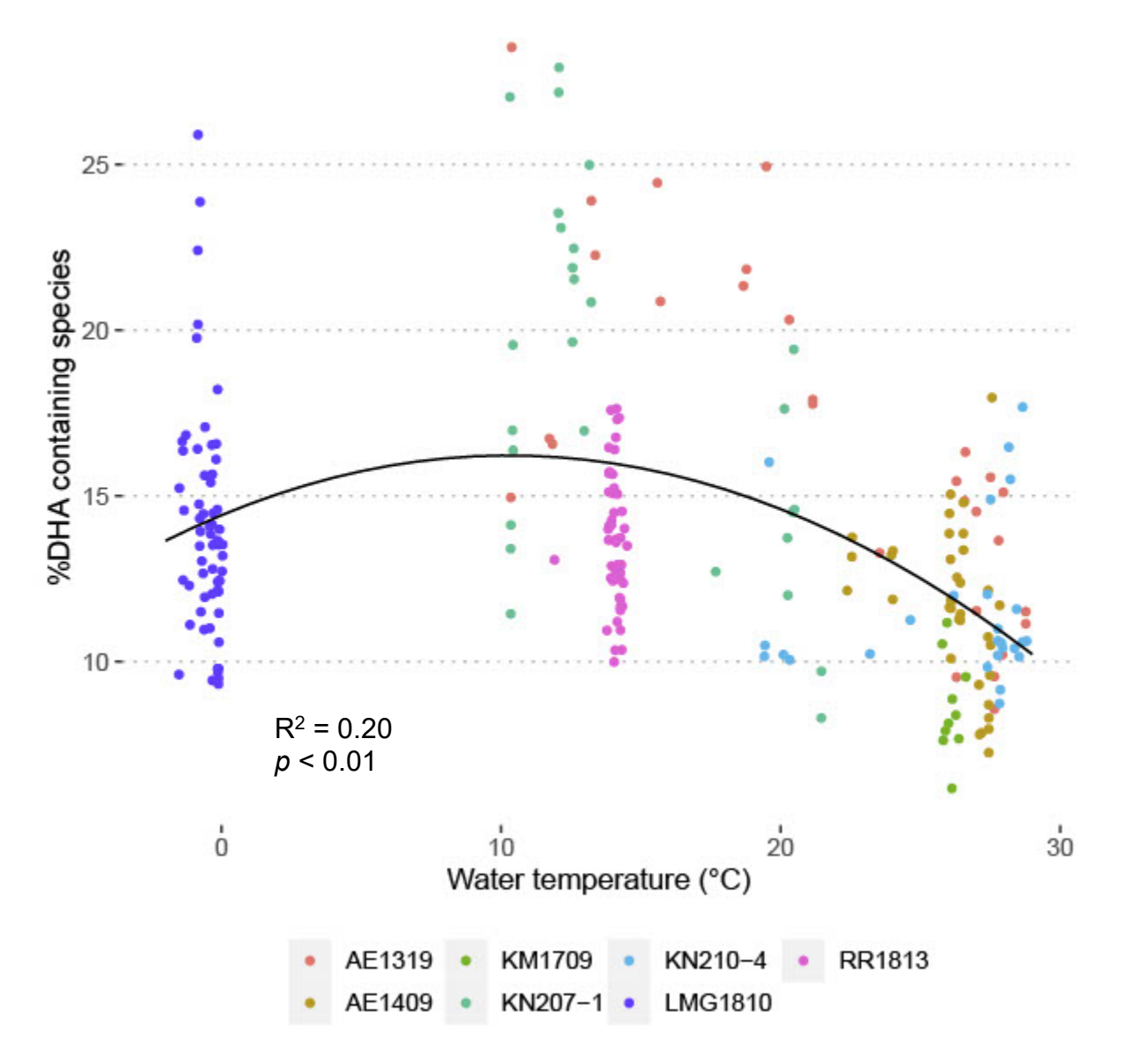


Figure. S5. Abundance of DHA containing membrane lipids versus temperature in mixed layer.Percent abundance of all membrane lipids containing a DHA fatty acid in mixed layer samples versus temperature. Seawater temperature at the time of sample collection is shown on the x-axis. Color denotes the deployment on which the sample was collected. Black line shows fitted values. Statistics for polynomial regression fit with ordinary least squares are shown in plot (n = 242, p values from F-test). (See Table S2 for full fit parameters).

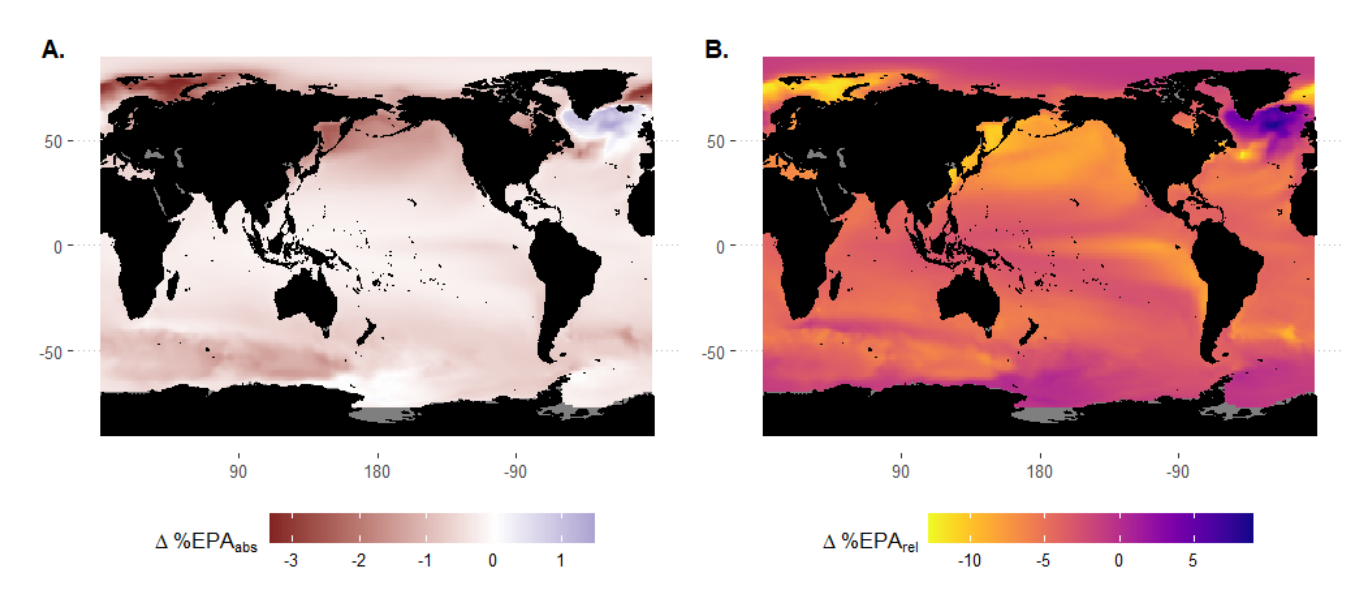
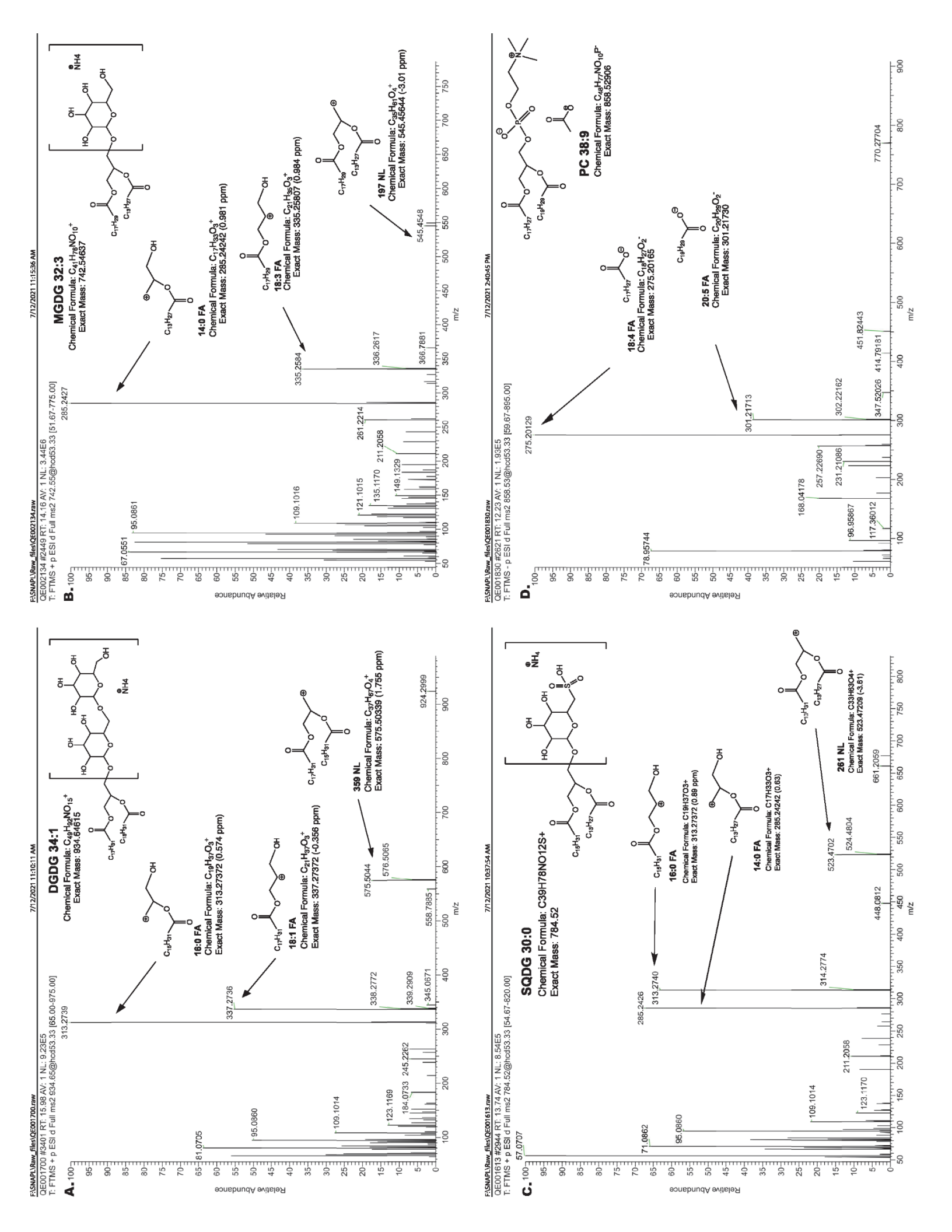
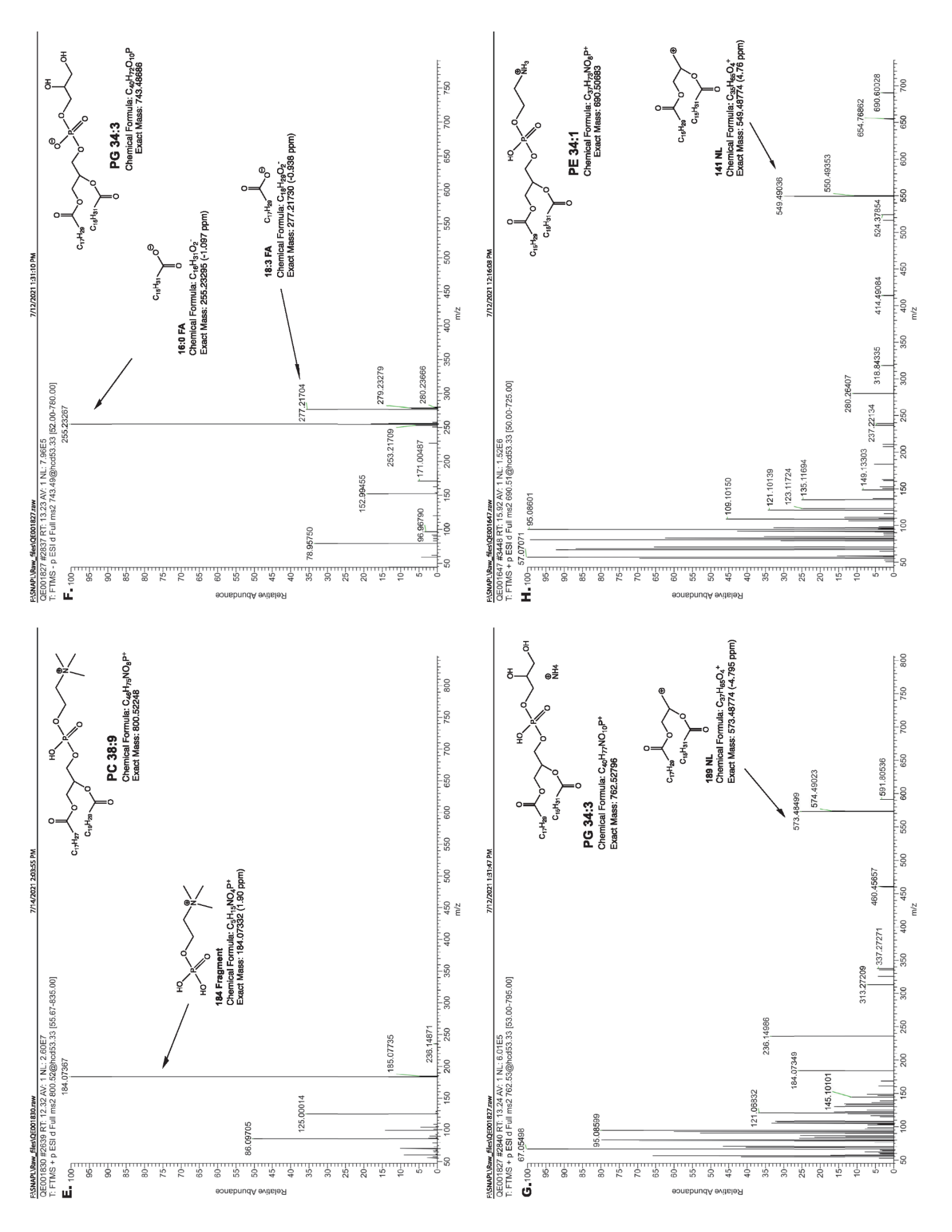
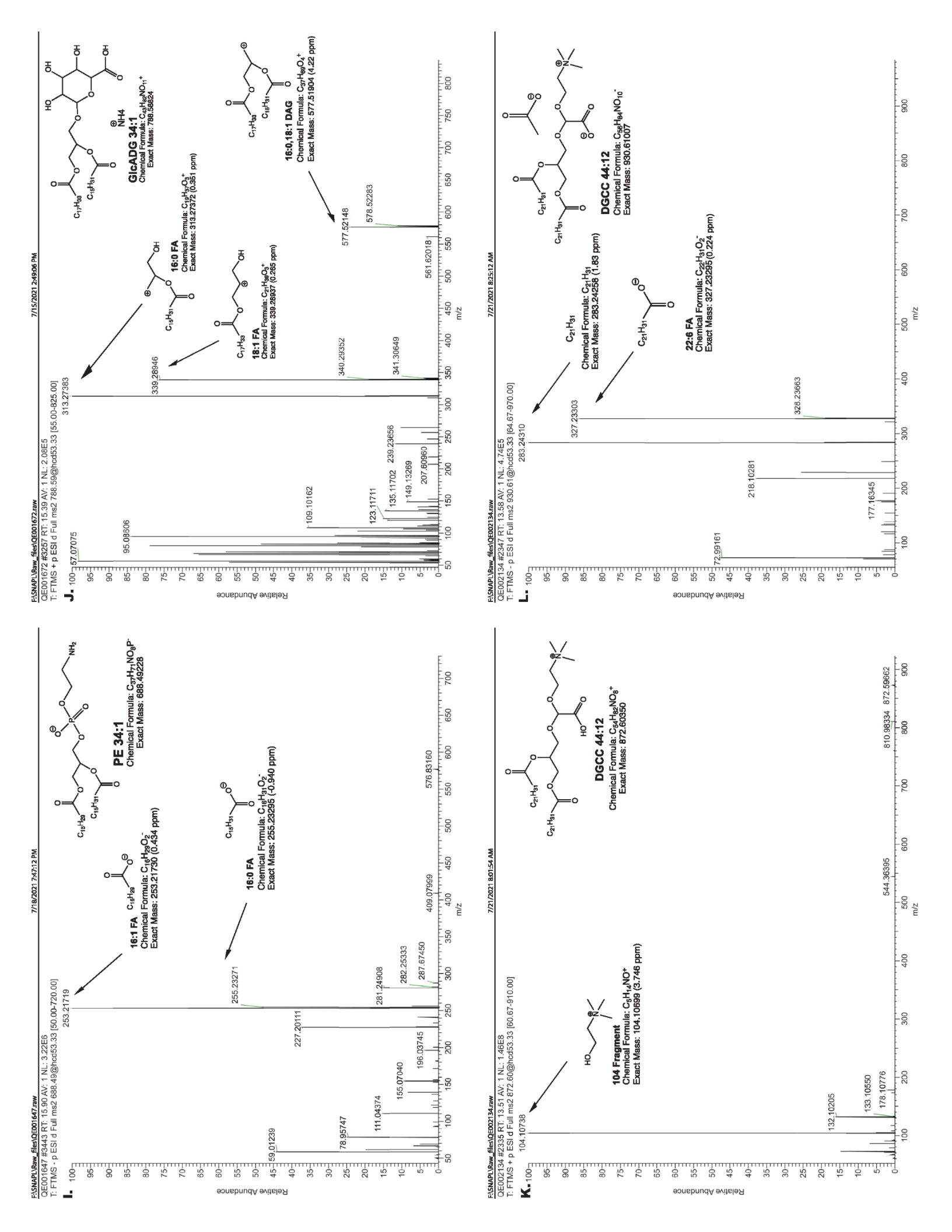
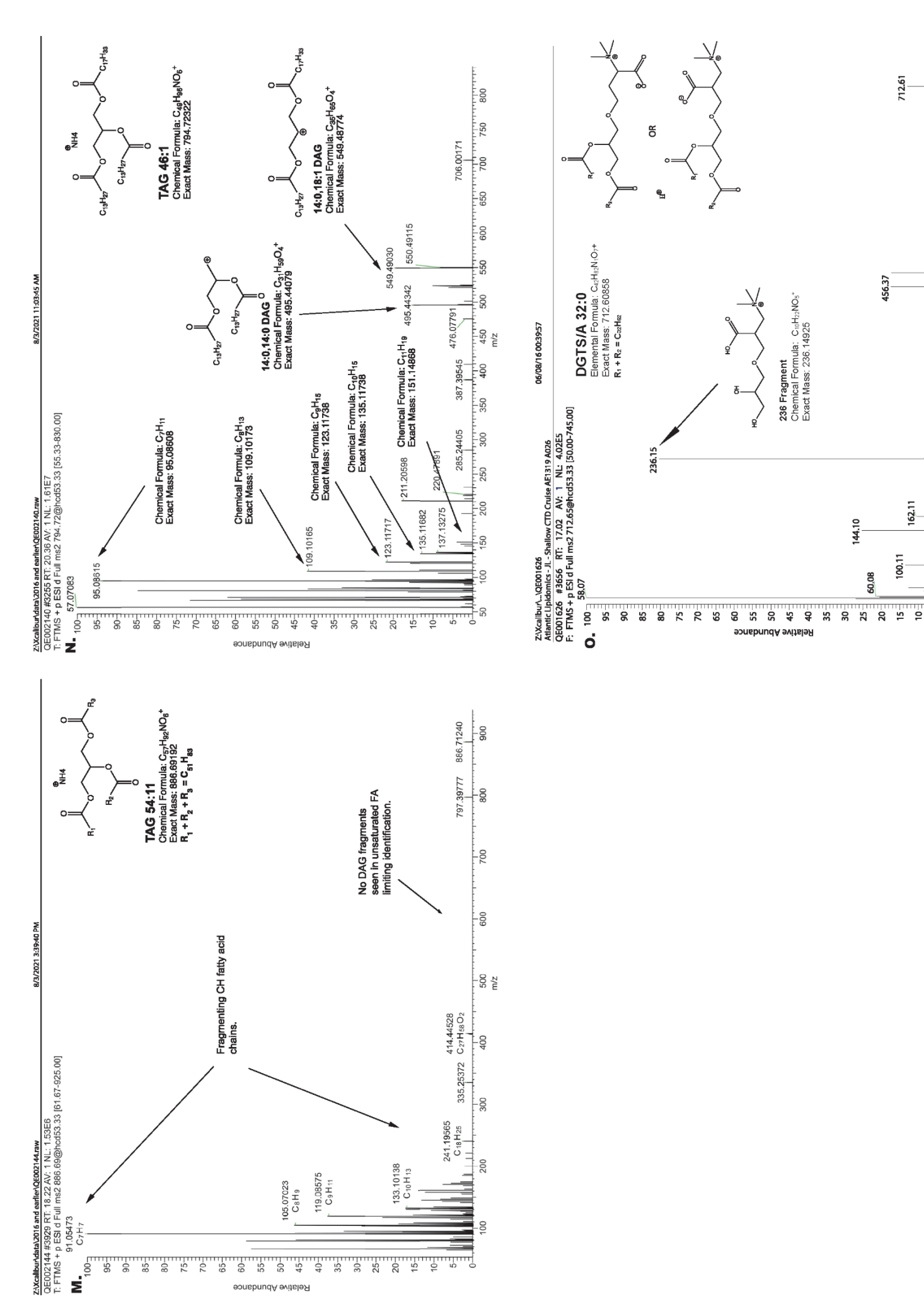


Figure. S6. Change in %EPA under SSP1-2.6 scenario. (A) Change in absolute %EPA (Δ %EPA_{abs}) at end of century from today using SST under SSP1-2.6 scenario (2080-2099) in the same model means at the SSP5-8.5 senario. (B) Change in relative %EPA (Δ %EPA_{rel}) as a ratio of Δ %EPA_{abs} to present day composition (1995-2014 %EPA).









m/z

196.38

543.05

446,35

Figure. S7.

Diagnostic MS² **Scans.** MS² spectra illustrating diagnostic fragments and neutral losses for each lipid class examined are shown here from samples within the dataset. Each subfigure lists the assignment for the feature (using the format of lipid class followed by fatty acid carbon number and number of fatty acid unsaturations separated by a colon), the chemical formula for the assignment, and the exact mass of the assignment. These are shown for each relevant fragment with the mass error (ppm) between the observed fragment and expected fragment in each scan. The abbreviation "NL" is used to designate a fragment resulting from a consistent neutral loss for a lipid class. Diagnostic fragments from lipid head groups are labeled with the nominal mass. A representative feature for each class is shown: **(A)** DGDG, **(B)** MGDG, **(C)** SQDG, **(D, E)** PC, **(F, G)** PG, **(H, I)** PE, **(J)** GlcADG, **(K, L)** DGCC, **(M, N)** TAG, and **(O)** DGTS/A. Negative mode MS² scans are also shown for species in which negative mode is used to identify fatty acid fragments. Positive mode scans from both a monosaturated and polyunsaturated TAG are shown to illustrate differences in fragmentation.

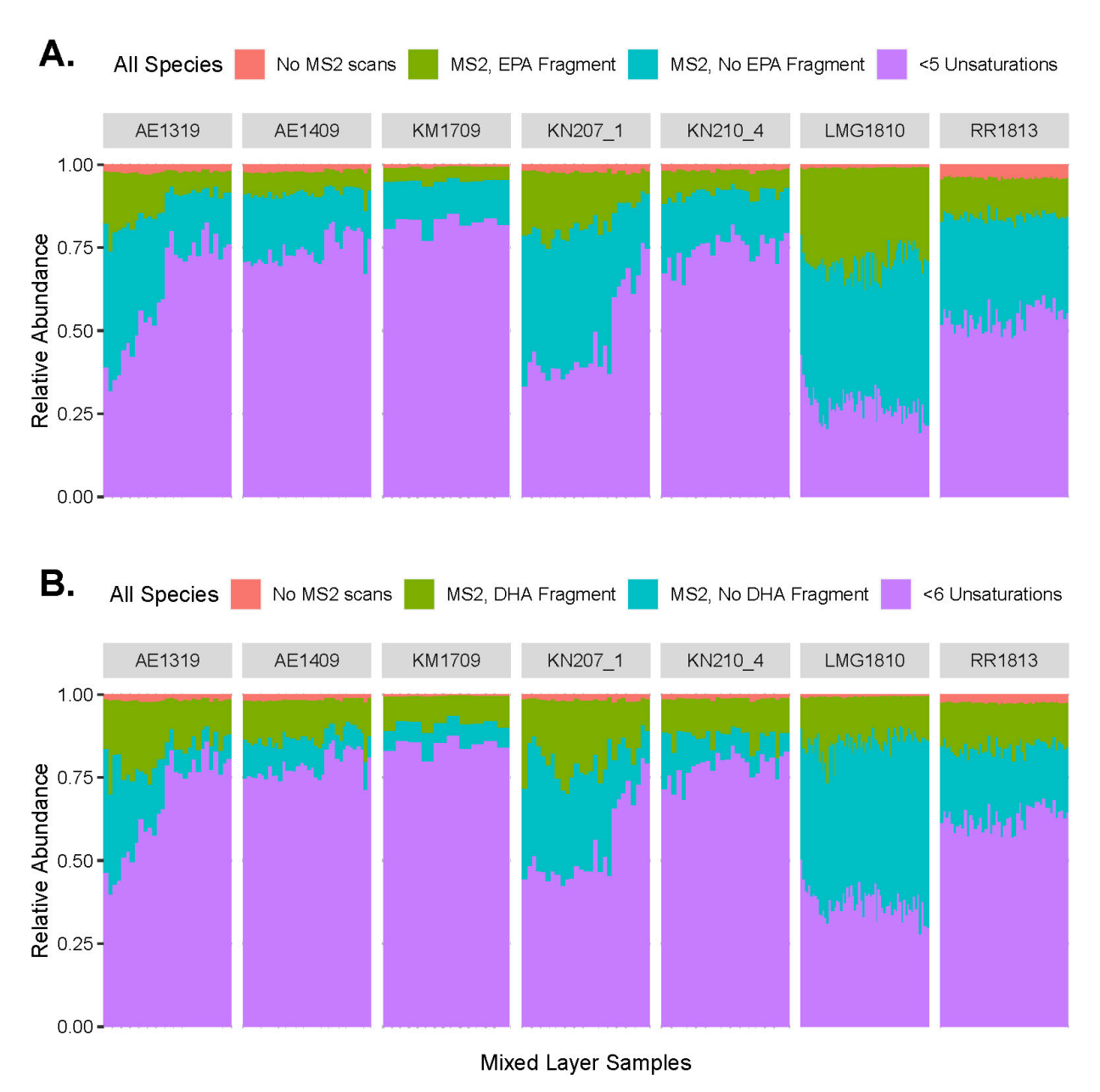


Figure. S8.Stacked bar graph of the percent abundance of membrane lipid species sorted by FA identification. Lipid species are sorted into four categories based on FA identification level for (A) EPA and (B) DHA. The percent abundance of lipid species annotations with fewer total unsaturations (< 5 or 6 unsaturations) than the LCEFA in question are shown in purple. The abundance of species for which a MS² scan was observed but no LCEFA fragment was seen are shown in blue. The abundance of species for which a LCEFA MS² fragment was observed are shown in green. The abundance of species with > 5 or 6 total unsaturations and no corresponding MS² scan are shown in red. Samples are grouped along the x-axis by cruise. Only samples from within the mixed layer are shown for each cruise.

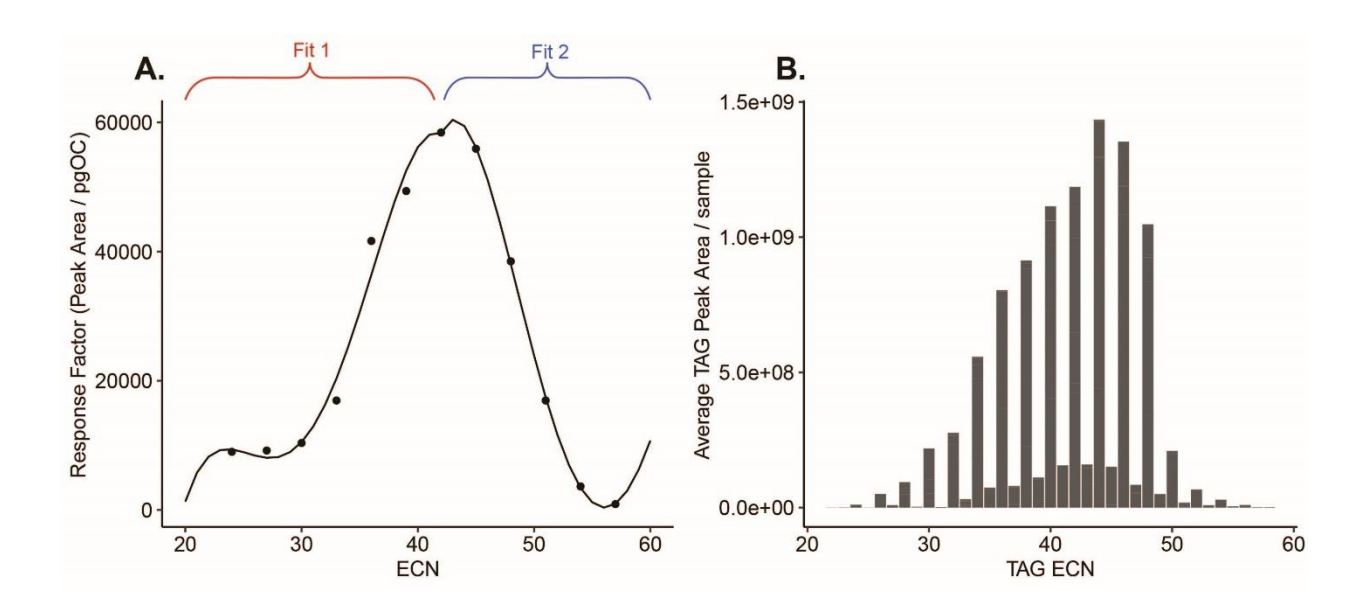


Figure. S9. Triglyceride response factor calibration. (A) The response factor (Peak Area / pg on-column) of different triglyceride (TAG) standards plotted against the standard's equivalent carbon number (ECN). ECN is defined as the number of carbons in the fatty acid chains minus two times the number of unsaturations (ECN = C - 2*U). Two quadratic functions were fit to this plot in order to predict the response factor of any TAG from its ECN. Fit 1 uses TAG standards with ECN of 2442 and Fit 2 uses TAG standards with ECN of 4257. TAGs with ECN < 42 were

corrected with Fit 1, those with ECN \geq 42 with Fit 2. **(B)** A histogram showing the ECN of

detected lipid species versus their average peak area in the dataset.

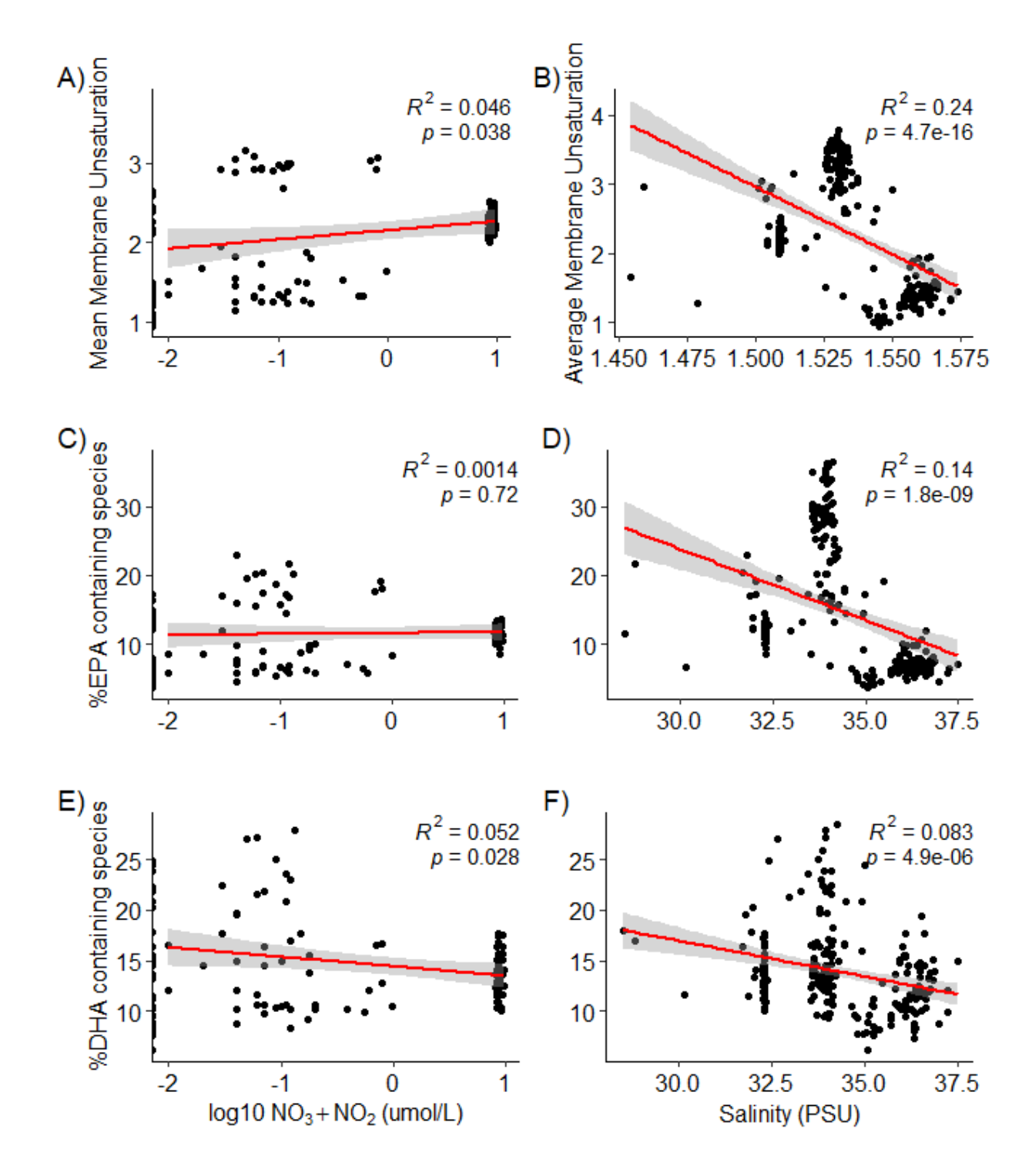


Figure. S10. Mean unsaturation and LCEFA content verses salinity and dissolved NO₃+NO₂. Mean unsaturation of all membrane lipids (A, B), %EPA (C, D), and %DHA (E, F) are plotted against salinity (n = 242) and dissolved NO₃+NO₂ (n = 115) respectively. Red line shows linear fit; inset shows coefficient of determination for linear regression with ordinary least squares and p value from F-test. Grey range shows 95% confidence interval of fit based on standard error.

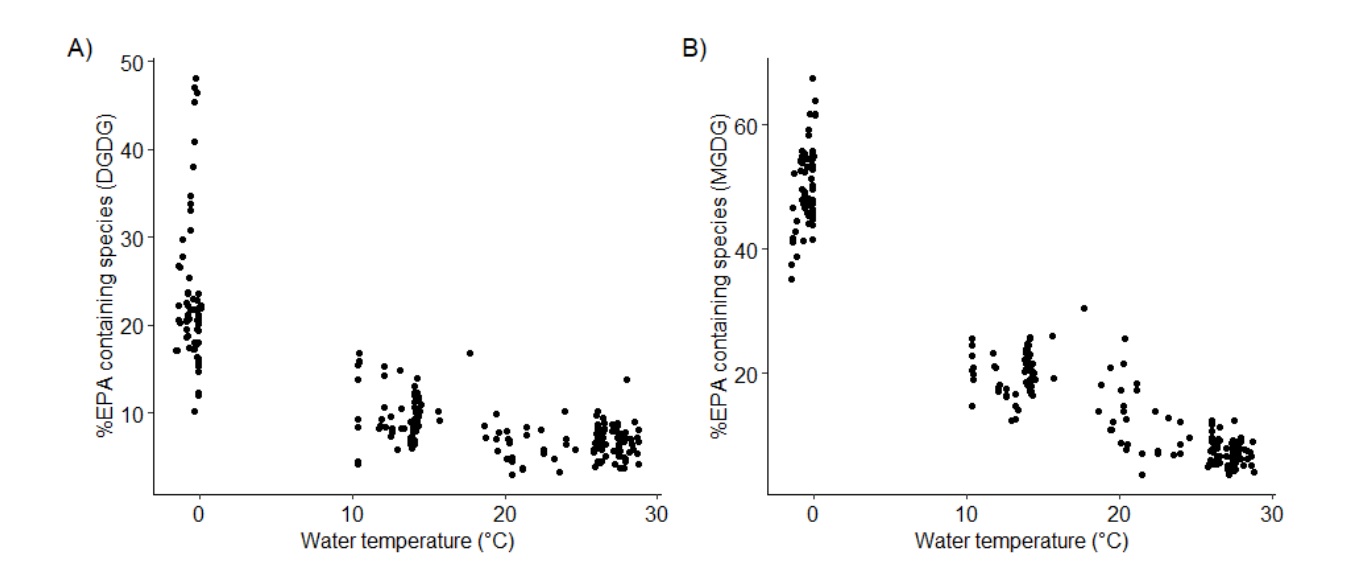


Figure. S11.
%EPA content of (A) DGDG and (B) MGDG verses water temperature. The y-axis shows the percent of DGDG or MGDG species that contained an EPA moiety. The x-axis shows water temperature. Only mixed layer samples are shown.

Table S1.

Linear regressions for weighted mean unsaturation per FA to temperature for each lipid class. For each lipid class, linear least squares regression was used calculate the linear fit between the weighted mean unsaturation of each sample (see methods 1.6,Fig. 2, Fig. S1, and Fig. S2) and the seawater temperature at time of collection. For each class, the adjusted R², coefficients, and p-value (F-test) are reported along with the number of species for each class in the dataset.

Lipid Class	Adjusted	Slope (m)	y-intercept	p-value	# of
_	\mathbb{R}^2				Species
SQDG	0.92	-0.0649	2.274	1.20E-133	96
DGDG	0.93	-0.0685	3.698	1.50E-143	67
MGDG	0.93	-0.1033	3.997	1.57E-141	85
GlcADG	0.72	-0.0183	1.089	3.21E-68	17
PE	0.85	-0.0674	2.796	2.00E-101	108
PC	0.92	-0.0489	4.524	1.57E-134	89
PG	0.91	-0.0280	1.478	2.99E-127	85
DGCC	0.85	-0.0527	4.516	3.02E-99	84
DGTS_DGTA	0.84	-0.0632	3.757	7.08E-98	167
TAG	0.80	-0.0596	3.026	2.28E-86	352
All Membrane	0.93	-0.0768	3.420	2.75E-138	798
Lipids					
All Lipids	0.89	-0.0667	3.175	3.34E-117	1150

Table S2. Quadratic model fits for %EPA and %DHA in membrane lipids to temperature as well as %TAG species with \geq 5 unsaturations to temperature. The adjusted R², coefficients, and p-value (F-test overall model) are reported. Both %EPA and %DHA of a sample were calculated as the combined abundance of membrane lipids with a positive or negative MS² scan that contained a LCEFA fragment in at least one representative MS/MS scan (see Methods 1.4, Fig. S8).

Fatty Acid	Adjusted R ²			Coefficient 3	p-
		(\mathbf{x}^2)	(x)	(b)	value
EPA	0.91	0.0183	-1.3001	28.0233	< 0.01
DHA	0.20	-0.0171	0.3510	14.4180	< 0.01
TAG species ≥5	0.82	-0.0414	-0.5985	79.6627	< 0.01
Unsaturations					

Table S3. Eluant gradient settings for HPLC analysis.

Time (min)	Flow (mL / min)	A (%)	B (%)
0.00	0.4	45	55
1.00	0.4	45	55
4.00	0.4	35	65
4.01	0.4	25	75
12.00	0.4	11	89
15.00	0.4	1	99
30.00	0.4	1	99
30.01	0.4	45	55
40.00	0.4	45	55

(See separate file.)

Table S4.

XCMS, CAMERA, and LOBSTAH settings for the peak detection, grouping, retention time correction, and annotation. Parameters are listed along with their settings, corresponding methods (Method), R software package (package), and reason for employing it (purpose).

Table S5. Lipid standards used in curves for quantification of lipid classes. The 'Used to Quantify' column contains all classes quantified with a given standard. The slope of the linear curve (Peak Area/pgOC) as well as the ratio of that slope to the DNP-PE reference standard (Response Relative to DNP-PE curve) is also reported. A range of response factors was used for TAGs (see Methods 1.5)

Standard	Supplier	Used to Quantify	Peak Area/pgOC	Response Relative to DNP- PE curve
DNPPE	Avanti Polar Lipids	NA	48,975	1.000
DGTS-d9	Avanti Polar Lipids	DGCC (diacylglyceryl-3- <i>O</i> -carboxyhydroxymethylcholine) DGTS (diacylglyceryl trimethylhomoserines) DGTA (diacylglyceryl hydroxymethyl- trimethyl-β-alanine)	257,151	5.251
15:0-18:1 PE-d7	Avanti Polar Lipids	Phosphatidylethanolamine (PE)	71,517	1.460
15:0-18:1 PC-d7	Avanti Polar Lipids	Phosphatidylcholine (PC)	131,852	2.692
16:0-18:1 PG-d5	Avanti Polar Lipids	Phosphatidylglycerol (PG)	61,195	1.250
MGDG 36:0	Avanti Polar Lipids	Monogalactosyldiacylglycerol (MGDG) Glucuronic acid diacylglycerol (GlcADG)	99,125	2.024
SQDG 34:3	Avanti Polar Lipids	Sulfoquinovosyl diacylglycerol (SQDG)	31,193	0.637
DGDG 36:4	Avanti Polar Lipids	Digalactosyldiacylglycerols (DGDG)	16,232	0.331
TAG Mix	Avanti Polar Lipids	Triacylglycerides (TAG)	362 to 60,412	0.007 to 1.234

(See separate file.)

Table S6.

Model output and statistics for environmental CTD predictor variables modeling weighted mean unsaturation of all membrane lipids, percent EPA containing lipids (%EPA), and percent DHA containing lipids (%DHA) within mixed layer samples.